Anna Peter, BSc

Crystal Shape Tuning in a Continuously Operated Crystallization Process

MASTER'S THESIS

to achieve the university degree of

Diplom-Ingenieurin

Master's degree programme: Chemical and Process Engineering

submitted to

Graz University of Technology

Supervisor

Ass.Prof. DI Dr. Heidrun Gruber-Wölfler
DI Peter Neugebauer

Institute of Process and Particle Engineering

Mag. Corinna Gressl
RCPE GmbH

Graz, March 2017

AFFIDAVIT

I declare that I have authored this thesis independently, that I have not used other than the declared sources/resources, and that I have explicitly indicated all material which has been quoted either literally or by content from the sources used. The text document uploaded to TUGRAZonline is identical to the present master‘s thesis.

Date

Signature

Acknowledgment

I would like to thank my internal supervisor Peter Neugebauer for his time and help and for the fun we had working in the lab! ☺ Thanks to the RCPE GmbH, where this work was carried out, and to Corinna Gressl, who was my supervisor at RCPE. Thank you, Heidrun Gruber-Wölfler, for becoming my official supervisor at the university!

Abstract

The aim of this work was the development of a tubular, continuous crystallization setup to modify the shape of acetylsalicylic acid crystals by using cycles of dissolution and growth. Crystal shape is a large field of interest, since it is known that properties of a crystal are often specific to a certain crystal face. Crystal shape can influence all downstream processes in the production, as well as characteristics like solubility, wettability or flowability. Research in the field of crystal shape enhancement and crystal property optimization is therefore of great importance.

The temperature cycling process investigated in this work was enabled by coiling a 50 meter long tube alternatingly in two water baths with different temperatures. Different solvents were used in the so-called chemical route experiments, where supersaturation-difference and percentage amount of seed crystals were kept constant. In non-chemical route experiments the supersaturation-difference was increased for a certain solvent and the outcome of the different supersaturation-differences were compared. An image analysis tool was used for evaluation and comparison of seed and product crystals. The chemical route experiments led to significant results and show the dependence of shape on the polarity of the solvent. The non-chemical route experiments overall showed the expected results, but did only achieve significant differences for one setting. For gaining significant results and changes of crystal shape in all non-chemical route experiments, the experimental setup has to be adapted in order to facilitate supersaturation-differences that are big enough to reach the desired modification.

Kurzfassung

Ziel dieser Arbeit war die Entwicklung eines kontinuierlichen Schlauch-Kristallisators, mit dem die äußere Form von Acetysalicylsäure-Kristallen, ihr Habitus, verändert werden sollte. Dafür wurde eine Methode verwendet, die die Kristalle abwechselnd durch Bereiche schickt, in denen sie wachsen oder angelöst werden.

Seit man herausgefunden hat, dass viele Eigenschaften eines Kristalls besonders ausgeprägt sind, wenn eine bestimmte Seite des Kristalls verhältnismäßig groß ist, hat der Habitus von Kristallen besonderes Forschungsinteresse erweckt. Der Habitus kann alle der Kristallisation nachgelagerten Prozessschritte beeinflussen. Auch Eigenschaften wie Löslichkeit, Benetzbarkeit oder Fließfähigkeit der Kristalle sind oft von der äußeren Form der Kristalle abhängig. Die Optimierung von Habitus und Kristalleigenschaften ist dadurch auch von großem Interesse für die Industrie.

Der in dieser Arbeit verwendete, sogenannte Temperature-Cycling Prozess besteht aus einem 50m-langen Schlauch, der alternierend in zwei Wasserbädern mit unterschiedlicher Temperatur aufgerollt ist. Durchgeführt wurden zwei Arten von Experimenten – die sogenannten „chemical route“ und die sogenannten „non-chemical route“ Experimente. Für die chemical route Experimente wurden verschiedene Lösungsmittel verwendet, während die Übersättigungs-Differenz und die prozentuelle Menge der Seed-Kristalle konstant blieb. In den non-chemical route Experimenten wurde nur die Übersättigungs-Differenz vergrößert. Für die Evaluierung der Kristalle wurde ein Bildanalyse-System verwendet.

Die Ergebnisse der chemical route Experimente zeigen signifikante Unterschiede und die Abhängigkeit des Habitus von der Polarität des Lösungsmittels. Die non-chemical route Experimente zeigen zwar im Mittel einen konsistenten Trend, signifikante Unterschiede unter Verwendung eines t-Tests konnten aber nur für eine Einstellung erreicht werden. Um signifikante Veränderungen des Habitus für non-chemical route Experimente zu erzielen, müssen höhere Übersättigungs-Differenzen in Schlauchkristallisator ermöglicht werden.

Contents

Acknowledgment I

Abstract II

Kurzfassung III

Abbreviations VII

1 Introduction 1

2 Theory of Crystallization 3

2.1 Cooling Crystallization 4

2.2 Batch versus Continuous Crystallization 4

2.3 Continuous Crystallizer Types 5

2.3.1 Forced Circulation Crystallizer 7

2.3.2 Draft Tube Baffle (DTB) Crystallizer 7

2.3.3 Fluidized Bed – Oslo Type Crystallizer 8

2.3.4 NiTech® Crystallizer 9

2.4 Crystal Structure 10

2.4.1 Crystal Planes 11

2.4.2 Growth Mechanisms & Surface Sites of a Crystal 11

2.4.3 Crystal Growth of Acetylsalicylic Acid (ASA) 13

2.5 Crystal Habit 14

2.5.1 Influences and Possibilities of Modification 14

2.5.2 Temperature Cycling 14

3 Aims of the Experimental Work 17

4 Materials and Methods 18

4.1 Materials 18

4.1.1 Solute 18

4.1.2 Solvents 18

4.2 Process Equipment 21

4.2.1 Equipment for Cycling Experiments 21
4.2.2 Equipment for Product Analysis 22
4.3 Experimental Methods 22
4.3.1 Determination of Solubility Curves 23
4.3.2 Preliminary Experiments 23
4.3.3 Experimental Setup 24
4.3.4 Stability of Seeds 28
4.4 Choice of Seeds – Amount and Size 29
4.4.1 Temperature Range 30
4.4.2 Calculation of the Supersaturation 30
4.4.3 Design of Experiments 32
4.4.4 Analysis 34
5 Results & Discussion 39
5.1 Results of Preliminary Experiments 39
5.1.1 EtOH 99.8% 39
5.1.2 EtOH 96% 40
5.1.3 Isopropanol 40
5.1.4 Acetone 41
5.1.5 Deionized Water 41
5.1.6 1-Hexanol 41
5.1.7 n-Heptane 42
5.2 Summary of Solubility Data 44
5.3 Stability of Seeds 45
5.3.1 Size and Amount 45
5.3.2 Habit 45
5.3.3 Crystal Structure 46
5.4 Residence Time 47

5.5 High Speed Camera Analysis 48
5.6 SEM Images 48
5.7 Results of the Main Experiments 49
5.7.1 Comparison of Chemical Route Cycling Experiments at ΔS_1 49
5.7.2 Comparison of Non-Chemical Route Cycling Experiments 55
5.8 Discussion 66
5.8.1 Considerations about Continuous Operation 66
5.8.2 ASA Growth and Dissolution Behavior 66
5.8.3 Challenges within this Work 67
5.8.4 Why did Non-Chemical Route Experiments not Achieve Significant Shape Changes? 69
5.8.5 Evaluation of Crystal Shape Change via Aspect Ratio 70
6 Conclusion and Outlook 71
Bibliography 74
Table of Figures 77
Table of Tables 80
Appendix i

Abbreviations

a	Aspect ratio
API	Active pharmaceutical ingredient
ASA	Acetylsalicylic acid
CL	Confidence level
CMR agent	Carcinogenic, mutagenic, reprotoxic agent
CSD	Crystal size distribution
CSTR	Continuous stirred tank reactor
DTB	Draft tube baffle
EtOH	Ethanol
F-faces	Flat faces
FBRM	Focused beam reflectance measurement
FC	Forced circulation
H_0	Null-hypothesis
H_a	Alternative hypothesis
HPLC	High-performance liquid chromatography
K-faces	Kinked faces
MSMPR	Mixed suspension mixed product removal
PFR	Plug-Flow reactor
PSD	Particle size distribution
Rel. Std.	Relative standard-deviation
rpm	Rounds per minute
S	Supersaturation
S-faces	Stepped faces
SEM	Scanning electron microscopy

Greek letters

ΔS	Supersaturation-difference
μ	Dynamic viscosity
ρ	Density

1 Introduction

In this study, a seeded, continuously operated tubular crystallizer is used to study the possibilities of changing a crystal's exterior appearance, its habit.

Crystallization is the second most important purification technique in chemical industry after distillation [1]. But not only purity is of importance anymore: In the last years, a large interest in crystal shape emerged due to the better understanding of crystal growth and crystallization methods. A crystal's habit can be of big importance, whenever there are special needs in the characteristics of the material. Food, pharmaceutical and electronics industry wish for materials with unique and enhanced properties and performance [2]. For crystalline materials, these properties are often specific to a certain crystal face and it is desired to maximize this face in comparison to the others [3].

A crystal's shape can have influence on its bulk transportability or flowability, its mechanical strength and on downstream processing, such as filtering, washing and drying [3]. It can also affect physical and chemical properties of the solid, such as solubility and dissolution rate [4], wettability, bioavailability [5] and catalytic activity depending on the relative size of a certain face [6].

For a long time, crystallization was carried out in batch-mode, where control of physical characteristics of the produced crystals and thus also process optimization was limited [4]. It is of big interest to develop continuous operating methods, which make it possible to influence the shape of a crystal according to one's needs. Work on this topic may be called "crystal shape tuning", which is what is aimed at in this study.

Previous work on this topic has mostly examined the effect of the choice of the solvent or the use of growth inhibiting additives [7]. This way of modification will be called **chemical route** in the following. A disadvantage of changing the solvent-composition or adding additives is, that it may need additional separation steps to remove these added substances, which may be uneconomical [8].

So-called **non-chemical routes** of crystal shape modification use the existing liquid system and aim to influence the crystal's habit only by adjusting the operating conditions. For example, the effect of different cooling modes on the supersaturation level and furthermore on the crystal habit can be examined [7]. In 2007, Snyder et al. theoretically introduced a new method of manipulating crystal growth, which is called temperature cycling and also is

a non-chemical route of crystal shape optimization. In this method cycles of dissolution and growth alternate with each other and thereby it is possible to obtain crystal shapes that could never have been reached only with dissolution or growth. [3], [6]

In this work, **acetylsalicylic acid (ASA)** was used as a model compound. Seed crystals were reshaped over the temperature cycling process. Different solvents and different supersaturations were studied; the chemical and the non-chemical route were investigated. No nucleation was considered, only the existing crystals were modified. Problems in continuous crystallizers, which approximate an ideal continuous stirred tank reactor, will be avoided by using a tubular crystallizer, approximating an ideal plug flow reactor. The special flow pattern inside the tubular crystallizer, called slug-flow, was created by introducing air bubbles into the suspension-flow and generating compartments. Every compartment is either filled with air or with seed suspension. With this method, it is ensured that every crystal has about the same residence time inside the crystallizer, because it is assumed that a crystal stays in its compartment from the inlet until the outlet.

The aim of the experiments was to get a better understanding of how factors such as supersaturation and solvent influence the habit of resulting crystals in a temperature cycling process. The terms habit, shape and morphology of a crystal are used as equivalent terms and refer to the outer appearance of a crystal.

The first chapter will contain state of the art theory on continuous crystallization and crystal shape enhancement. Then, equipment and materials used in this work will be presented, followed by a detailed description of the experimental methods that were applied. In the chapter “results and discussion” results of preliminary batch-experiments and first cycling-tests will be discussed, as well as the outcome of the main experiments with different solvents and different supersaturation-differences. Finally, challenges that were faced during the work, and additional thoughts concerning assumptions and evaluation will be discussed.

Another part of this work was the production of a defined amount of acetylsalicylic acid-crystals of different shape compared to the seed crystals for further research and measurements at the Research Center Pharmaceutical Engineering GmbH (RCPE). After it was figured out which settings led to the biggest shape change over the cycling process, one gram of the desired crystals was produced.

2 Theory of Crystallization

Crystallization is basically the transformation of an amorphous, liquid or gaseous material into a crystalline state. The most important application of crystallization is purification, where it is used as a thermal separation technique to obtain highly concentrated or even pure substances [9].

The driving force for nucleation and the growth of crystals is supersaturation. Supersaturation can be achieved in different ways, such as cooling, evaporation, changing the composition of the solvent or a chemical reaction. Figure 2-1 shows three of the before mentioned ways of reaching the supersaturation zone. State (A) in the diagram equals a stable condition of the solution in the unsaturated range. If this solution undergoes isothermal evaporation of the solvent, it eventually reaches a supersaturated state (B), where nucleation and growth of crystals can happen. If the solution of state (A) is cooled, it reaches a supersaturated state (C). If the solution is cooled and evaporated at the same time, it will reach a condition between (B) and (C), for example (D). The metastable zone is an area between saturation curve and supersaturation curve, above which birth of first nuclei is detected. Its width is very different for different liquid systems. This means that a solution can stay at a concentration above the saturation curve for some time, until it eventually starts to nucleate.

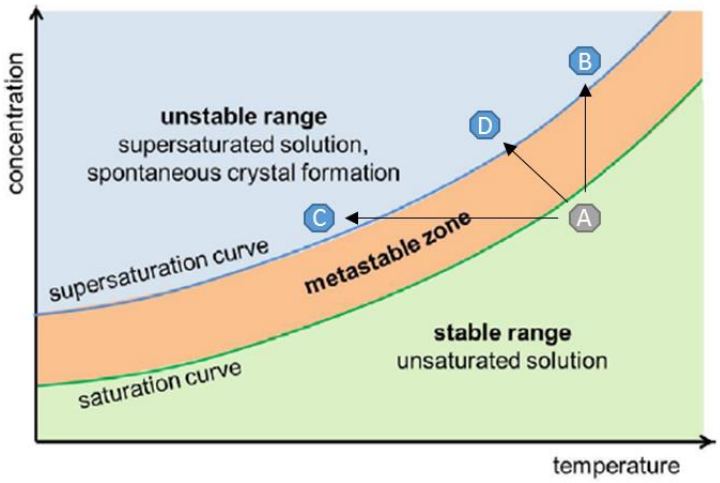

Figure 2-1: Different ways of reaching supersaturation zone from stable state (A): through isothermal evaporation (B), through cooling (C) or through cooling and evaporation (D) [11]

The six steps of an industrial crystallization process are

1. Supersaturation
2. Nucleation
3. Crystal growth
4. Stabilization of the crystals (if necessary)
5. Filtration
6. Drying

This work focuses on step 1 and 3. Supersaturation was achieved by cooling, which is why this type of crystallization is discussed in detail.

2.1 Cooling Crystallization

Cooling crystallization is recommended, whenever the solubility of the substance in its solvent increases with temperature. The solution is introduced into the crystallizer and then cooled either at a constant cooling rate or by varying the cooling rate in a way that a constant supersaturation is maintained. Using a constant cooling rate leads to very differing growth behavior. In the beginning either no growth-surface or only the small surface of a few seed crystals is available, leading to high supersaturation and a lot of nucleation. In the end of the cooling process, there is a lot of surface area available but due to the low supersaturation, which is left, crystal growth takes place very slowly. Mostly, the optimal supersaturation is the one, where the highest possible growth rate is facilitated while nucleation is kept as low as possible to obtain coarse crystals. [9]

2.2 Batch versus Continuous Crystallization

Today the ideal operation mode for every process seems to be a continuous and steady-state one. In crystallization (and also other unit operations) however, this is not always true. A batch-crystallizer has simpler equipment, less encrustation-problems on heat-exchangers and is often easier to control and more flexible. On the other hand, its operation costs are commonly much higher and a certain batch to batch variety of product quality cannot be avoided. Continuously operated crystallizers are generally smaller, more energy-efficient and produce constant product-quality. Disadvantages of continuous crystallizers are higher initial equipment costs and a lot of knowledge about the process being required. Because a continuous crystallizer is designed for a narrow range of conditions, it is also less flexible. [12], [13]

Usually the shut-down after every batch-process is regarded as a big disadvantage of batch operation. In crystallization however, especially in the pharmaceutical industry, it is also seen as a quality assurance because the thorough cleaning prevents contamination, in terms of seeding, of the next charge. In continuous crystallizers it often happens, that deposits self-seed the solution after a certain operating time. This is undesirable and often enforces an early shut-down and cleaning, which takes even more time than for the batch-mode, because of the much more complex setup of the continuous unit. A continuous crystallizer also often does not discharge its product under equilibrium conditions, which makes the presence of a holdup tank after the actual crystallization necessary to allow equilibrium to be approached. If no equilibrium is reached, problems within the next steps can arise due to possible further crystallization. Another problem can be that the following downstream processes are not continuously operated, which again makes holdup tanks necessary. Generally, one process characteristic to decide between continuous or batch production can be the production rate. If the production rate is high enough, continuous crystallizers are to be preferred over batch processes. The actual production rate that is necessary to make a continuous crystallizer economically advantageous, depends on the economic value of the material that is crystallized. [12], [13]

2.3 Continuous Crystallizer Types

The two ideal continuously operating reactor types are the continuous stirred tank reactor (CSTR) and the plug flow reactor (PFR). Both are characterized by a continuous flow of reactants and product. The CSTR assumes perfect backmixing and the same product concentration inside the reactor and at the outlet. Ideal plug flow behavior means that there is no longitudinal mixing (backmixing) but complete radial mixing within each plug. A plug can be considered an infinitesimal slice within the flow through any tube. Characteristic for a plug flow is an identical flow velocity and residence time of all particles within the reactor. Although no real reactor will behave exactly like the ideal one, the operating flow conditions can often approximate the ideal ones. [14]

In crystallization the CSTR is called mixed suspension mixed product removal (MSMPR) crystallizer. The MSMPR-crystallizer is assumed to have a uniform crystal size distribution (CSD) in every arbitrary small element of volume. In the ideal crystallizer, this CSD also exists in the product stream, which means that absolutely no product classification takes place at withdrawal. [14]

The influences on the behavior of an MSMPR crystallizer are shown in Figure 2-2. In the beginning, the supersaturation in the feed solution controls the amount of nucleation and growth. Whether existing crystals grow or new nuclei are born influences the CSD of the product crystals. The CSD inside the crystallizer determines the surface area that is available for growth. The surface area of the already existing crystals therefore again influences the variation of supersaturation inside the crystallizer. If new feed material enters and there is already a lot of crystal surface area (i.e. many small crystals) available, supersaturation will decrease very fast, because material will immediately grow onto the existing surface area. Therefore, probably no nucleation will appear. If the surface area of the crystals in the crystallizer is small (i.e. only a few, big crystals), supersaturation in the crystallizer will stay at a higher level, because there is not enough surface area for fast crystal growth. This will eventually lead to nucleation.

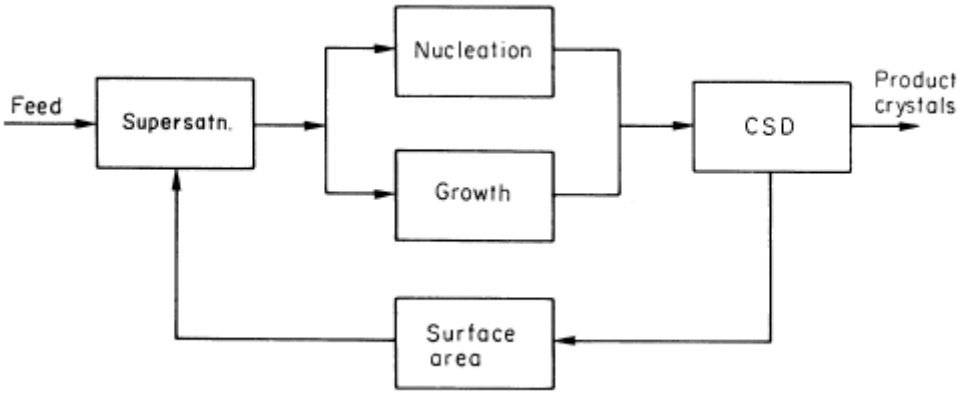

Figure 2-2: Information flow-diagram of a continuous MSMPR crystallizer [13]

A comparison of MSMPR and plug-flow crystallizers shows that in a MSMPR crystallizer temperatures are easier to control. Also, it is simple to replace parts of the system and maintenance is less complex. On the other hand, it typically is less efficient than a plug-flow crystallizer. The plug-flow crystallizer normally has a higher efficiency than an MSMPR crystallizer of the same volume and it can run for a long period of time without maintenance. However, maintenance is more expensive and more complicated and settling of solids and plugging are a big issue. [4]

A few continuous crystallizer types for industrial applications will be presented in the following.

2.3.1 Forced Circulation Crystallizer

The forced circulation (FC) crystallizer is classified as a MSMPR crystallizer. It is the least expensive type of continuous MSMPR crystallizers and is available in a large range of sizes. By a sufficient rate of circulation, supersaturation can be controlled and spontaneous nucleation and deposits on the walls can be avoided. Its only drawback is that the CSD of the generated crystals can hardly be influenced. Still it is one of the most frequently used crystallizers in industry. [15]

The FC crystallizer, shown in Figure 2-3, evaporates solvent, which increases supersaturation and leads to nucleation in the crystallizer vessel. Evaporated solvent is condensed and returned to the vessel. Slurry from the crystallizer vessel is circulated through the heat exchanger and returned to the crystallizer vessel, where its supersaturation is released and causes already present crystals to grow. Supersaturation is controlled by a sufficient circulation.

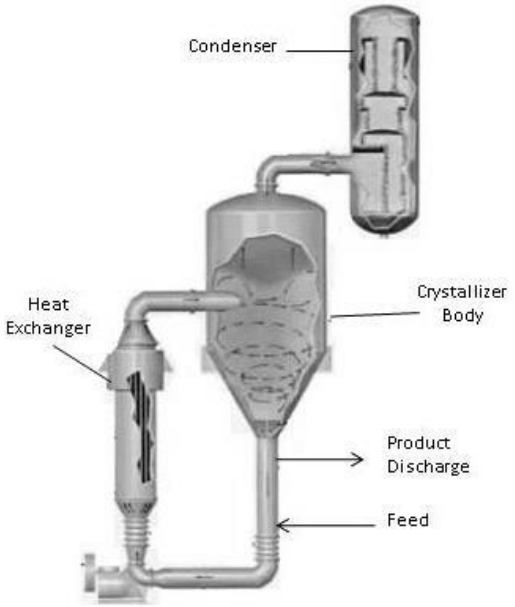

Figure 2-3: FC crystallizer represented schematically [15]

2.3.2 Draft Tube Baffle (DTB) Crystallizer

The Swenson DTB crystallizer is capable of producing larger crystals with a narrow CSD [13]. A sketch of this type is shown in Figure 2-4. Through a draft tube, growing crystals are transported from the lower parts to the top of the crystallizer, where supersaturation is highest because solvent is evaporated from the surface. Outside the tube crystals sink down again and are again sucked up into the tube until they are large enough to sediment past

the tube and finally reach the product discharge zone. Fines are withdrawn from a settling zone, dissolved and fed back into the crystallizer.

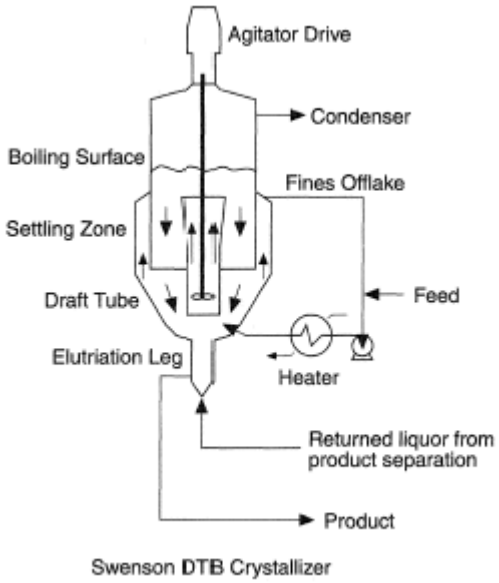

Figure 2-4: Swenson DTB crystallizer represented schematically [12]

2.3.3 Fluidized Bed – Oslo Type Crystallizer

Oslo-type crystallizers, also called classified-suspension crystallizers, produce a fluidized bed of crystals. Suspension of the crystals and agitation is provided by an external circulation loop of (either crystal magma or) a relatively crystal-free solution, which allows crystals to grow and minimizes secondary nucleation. [12], [13]

A spatial separation of supersaturation- and growth-zone is desired. Figure 2-5 shows a sketch of a fluidized bed-crystallizer. In a possibly crystal-free zone, the evaporation chamber, the solution is supersaturated, then conveyed to the growth zone, where it releases its supersaturation by giving the excess-solute to crystals and letting them grow. The growth zone is designed as a fluidized bed. An upward flow causes the crystals to stay in different heights according to their size. The bigger the crystal, the higher its sedimentation velocity and the faster it reaches the product outlet, which is located at the very bottom of the growth zone. In this way a relatively narrow crystal size distribution can be realized. The fluidized bed crystallizer can be operated as a cooling, evaporative or vacuum crystallizer. [9]

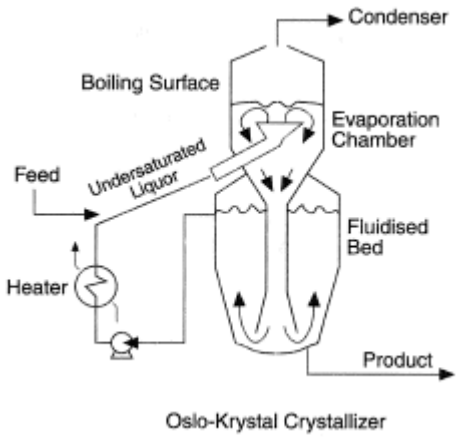

Figure 2-5: Oslo-Krystal crystallizer represented schematically [12]

2.3.4 NiTech® Crystallizer

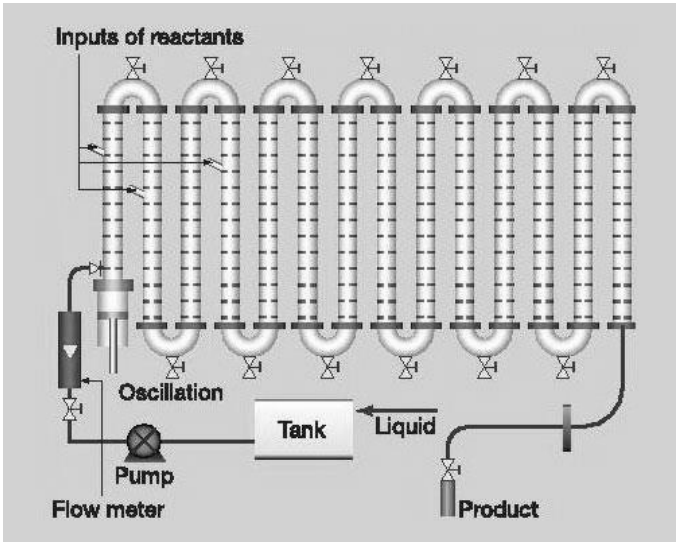

Figure 2-6: NiTech® reactor scheme [16]

The NiTech® crystallizer, shown schematically in Figure 2-6, is an example of a tubular crystallizer for cooling crystallization. It is basically a tube divided into sectors by baffles. Plug-flow mixing in each sector is achieved by flow oscillation. The crystallizer is available in different sizes, ranging from 7 to 20 metres in length and from 30 to 90 minutes of residence time at a nominal flow rate of 40 ml/min. It enables improved control over size and shape of crystals due to the increased specific area per volume for heat transfer together with the plug flow conditions. [17], [16]

2.4 Crystal Structure

Crystals are solids with a regular arrangement of their constituents. In the 19th century August Bravais introduced the concept of the unit cell, which is the smallest part of a crystal, which still possesses all characteristics of the lattice structure and its symmetric relationships. A unit cell is shown in Figure 2-7. It is specified by its lattice parameters a, b and c and the angles α, β and γ. In theory a crystal consist of its duplicated unit cell arranged side by side and on top of each other. Bravais stated that there are 14 different types of unit cells, called Bravais lattices, which can be assigned to seven crystal systems: cubic, tetragonal, orthorhombic, rhombohedral, hexagonal, monoclinic and triclinic. The different crystal systems have different relations between their lattice parameters. [11]

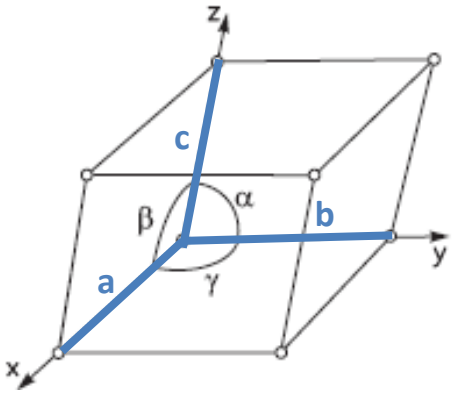

Figure 2-7: Unit cell with its lattice parameters [9]

As already mentioned, ASA was used as a model substance for this work. The unit cell of the common form I is shown in Figure 2-8 and consists of four asymmetrical molecules. It belongs to the monoclinic crystal system and its lattice parameters at 100 K are a= 11.23 Å, b= 6.54 Å, c= 11.23 Å, α=γ= 90°, β= 95.89° [28]. It belongs to the space group $P2_1/c$.

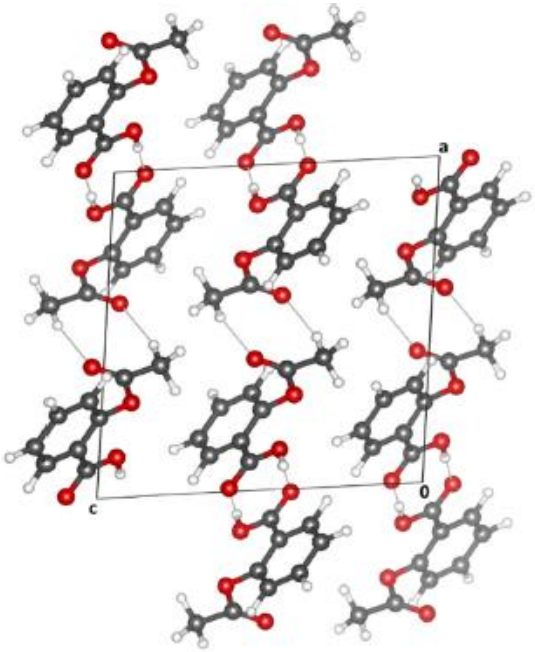

Figure 2-8: ASA unit cell [29]

2.4.1 Crystal Planes

Each crystal plane can be identified and described by the so-called Miller indices h, k and l, which are the smallest integer multiples of the reciprocal values of the axial intercepts. Figure 2-9 shows the indexing of an exemplary chosen plane within a unit cell. The Miller indices are usually written as (hkl). The depicted plane in the figure equals the (312)-plane. A plane at the surface of a crystal is also called crystal face and is of special importance because these faces define the habit of a crystal. [9]

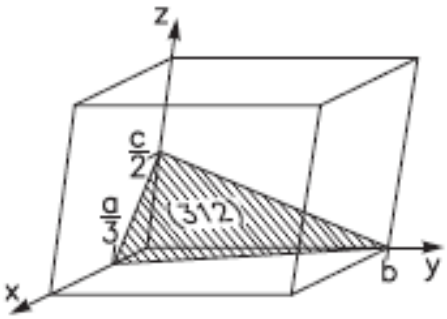

Figure 2-9: Using Miller indices to index a crystal plane [9]

2.4.2 Growth Mechanisms & Surface Sites of a Crystal

There are a lot of different crystal growth theories. Surface energy theories assume that a crystal grows to the shape in which it has a minimum surface energy. Diffusion theories

state that material is deposited continuously onto a crystal's face at a velocity proportional to the concentration difference between the crystal surface and the bulk of the solution. Adsorption layer theories on the other hand assume that crystal growth is a discontinuous process, taking place by adsorption in layer by layer manner. In this theory, crystal faces are shown to have flat surfaces, steps and kinks, as shown in Figure 2-10. On a flat surface a new molecule can only bind to one surface, on a step it can attach to two surfaces and on a kink at least three surfaces are available. Molecules are most easily incorporated into the crystal at a kink. Therefore, a face that is covered with kinks grows fastest, whereas a flat surface grows slowest. [13],[18],[2]

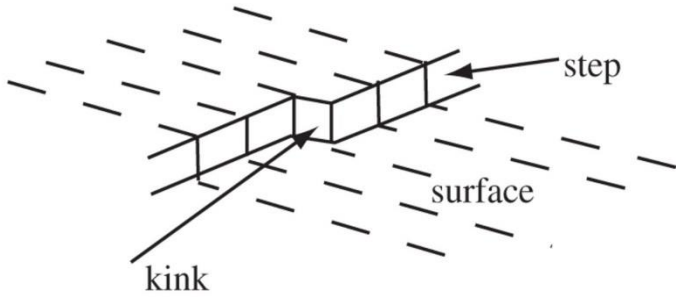

Figure 2-10: Surface sites of a crystal [18]

It was found that almost all crystals show dislocations. The screw dislocation, shown in Figure 2-11, has a big impact of a crystal's growth, since the crystal face can grow continuously "up a spiral staircase" [13].

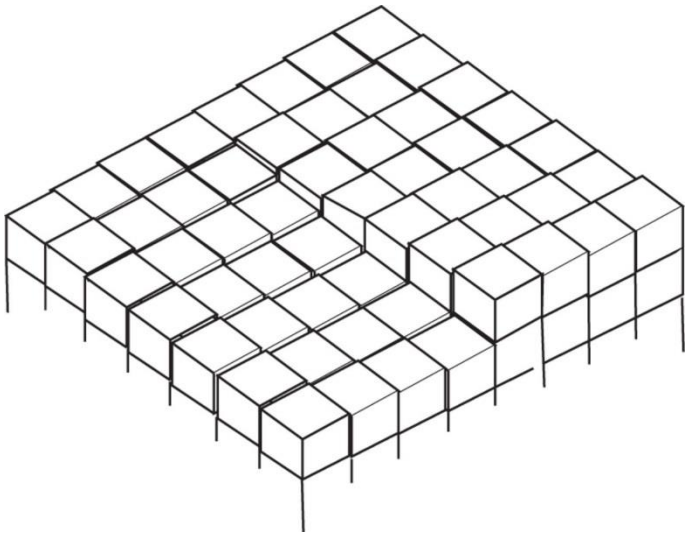

Figure 2-11: Screw dislocation on a crystal face [18]

2.4.3 Crystal Growth of Acetylsalicylic Acid (ASA)

The three major faces of an ASA-crystal are the (100)-, (010)- and the (001)-plane [19]. Research and simulation of Tomassone et al. [19], [20] showed that face (001) became the biggest face, when ASA was recrystallized from ethanol. When in contact with a polar solvent like ethanol, ASA-crystals are able to grow in the direction of their (100)- and (010)-face, whereas growth in (001)-direction is stunted. This leads to plate-shaped crystals. When recrystallized from a non-polar solvent like hexane, growth in (100)- and (001)-direction is inhibited, but in (010)-direction it is still facilitated. This leads to needle- or rod-shape. [21]

A dissolution study of the (100)- and (001)-faces by atomic force microscopy stated that plane (100) dissolves about six times faster than plane (001), under 0.5M HCl [22].

Surface characterization-studies of ASA crystal planes using molecular dynamics simulation studied the role of H-bonds on stabilizing ASA's crystal faces. The stability of the crystal faces in contact with two different solvents, ethanol and hexane, and the growth mechanisms were investigated. The (001)-face is populated with methyl and carboxyl groups. The molecules on the (001)-face lose their lattice structure completely, if they are not paired with other ASA molecules before contacting any solvent. Growth in this direction can therefore only happen in a layer-by-layer manner, which is kinetically unfavourable. The unpaired (100) surface of ASA is populated with OH-groups. Their hydrophilic nature prefers the interaction with a polar solvent and thus growth along this face is increased when in contact with ethanol. On the (010)-plane, the interlaced arrangement of hydrophilic hydroxyl groups and hydrophobic phenyl groups stabilizes the surface structure in both ethanol and hexane. Growth on the (010) surface is likely to happen via very fast single molecular addition, which is favoured thermodynamically and kinetically. [19]

The ability of a material to exist in different forms of crystal structure is called polymorphism. Until 2005 ASA was thought to have only one crystal structure and therefore no polymorphs. In 2005, a first report of a second polymorph was published [23]. Several critical voices arose, doubting the results [24]. Following studies showed crystals consisting of ‘‘an intergrowth of two polymorphic domains” [25]. Only in 2010 reports were published proving that crystals of pure form II were crystallized. Pure Form II was obtained when crystallized in the presence of aspirin anhydride in organic solvents; in the mentioned study acetonitrile and tetrahydrofuran were used. The crystals were stable for months under ambient conditions [26], [27]. The importance for pharmaceutical applications of this new

polymorphic form is presently limited due to its rare appearance. So far, information about differences in their physical properties are not found in literature.

2.5 Crystal Habit

The habit of a crystal is its exterior appearance. Although crystals can be associated with one of the seven general crystal systems, the relative sizes of the different crystal faces can vary widely, even though it is the same substance and polymorph. This variation is called modification of habit or change of shape. An example can be seen in Figure 2-12, where different habits of a crystal, belonging to the hexagonal system, are shown [13].

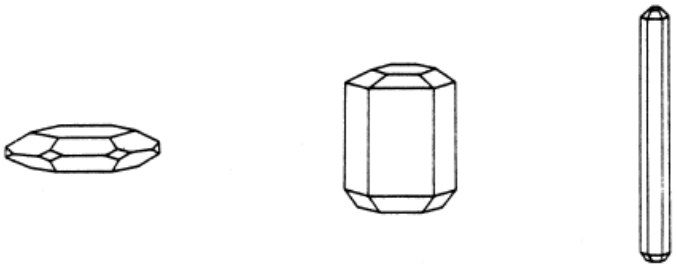

Figure 2-12: Different habits of a crystal of the hexagonal crystal system [13]

2.5.1 Influences and Possibilities of Modification

Modification of a crystal's habit can happen unintentionally for example because of impurities, which may increase or stunt growth in one or more directions. On the contrary these observations can also be used intentionally to modify the crystal's exterior in a way that it fits different requirements better.

The growth rates of different crystal faces are influenced on the one hand by internal factors such as the crystal structure, which determines the surface structure, and crystal defects, which are deviations from the theoretical structure. On the other hand growth is influenced by external factors like supersaturation, type of solvent, additives, solution composition, impurities and physical conditions like temperature, solution flow rates, electric and magnetic fields or ultrasound. [2]

2.5.2 Temperature Cycling

A method that uses the influence of temperature on a crystal's shape, is temperature cycling. In this method, a crystals alternatingly pass hot and cold regions and therefore are exposed to cycles of dissolution and growth. Growing crystals always move towards a

steady-state shape, whereas dissolving crystals move away from a steady-state shape. This means that by switching between dissolution and growth, it is possible to obtain crystal planes and subsequently shapes that could never have formed with growth alone [6].

The shape of a crystal can only be changed by cycling, if the relative rates of growth and dissolution of a certain face are anisotropic, which can be the case because of differences in growth mechanisms, asymmetry in super-/undersaturation or the use of surface active additives.

Figure 2-13 shows a model-system, where 20% of the crystal are dissolved in each cycle and the crystal is always regrown to its original volume. In this case only one face is considered to have different velocities of growth and dissolution and the growth velocity is defined to be bigger than the dissolution velocity. The crystal shows a maximum in sphericity for the most cubic habit after about 30 cycles.

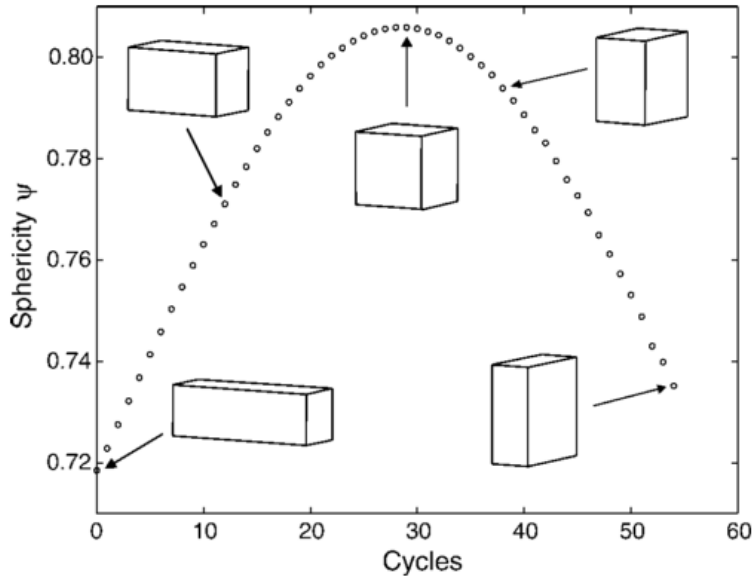

Figure 2-13: Change of crystal habit and sphericity through temperature cycling if growth velocity is bigger than dissolution velocity [3]

If the dissolution velocity of the same face as before is bigger than its growth velocity, habit and sphericity of the illustrative system change according to Figure 2-14. The crystal is elongated over the cycling process, leading to a smaller sphericity.

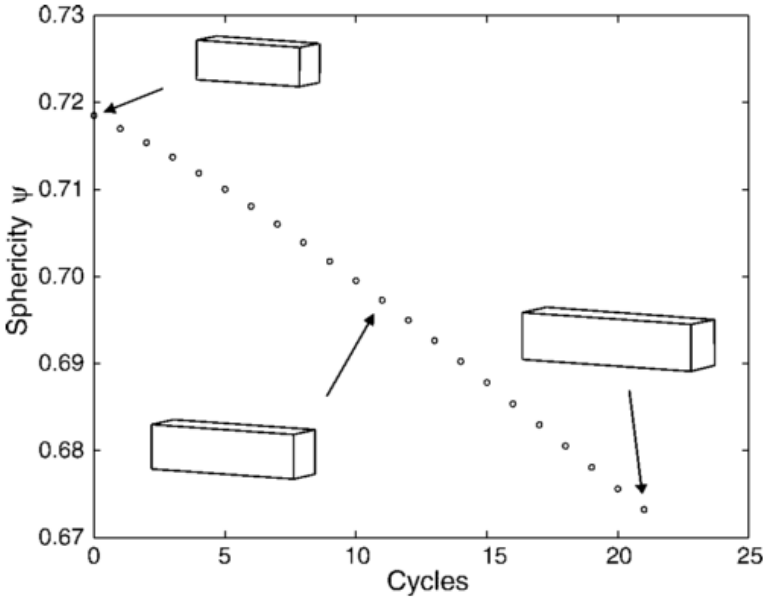

Figure 2-14: Change of crystal habit and sphericity through temperature cycling if dissolution velocity is bigger than growth velocity [3]

Even if growth and dissolution velocity are the same for every crystal face, the habit can change, if the crystal is dissolved to an extent where certain steady-state growth faces disappear. In the illustrative system, faces disappear if about 65% of the crystal's material is dissolved in the dissolution step. In Figure 2-15 starting (left) and product crystal (right) are shown. The product crystal has lost its (100)- and (001)-face and instead face (101) appeared and became the biggest.

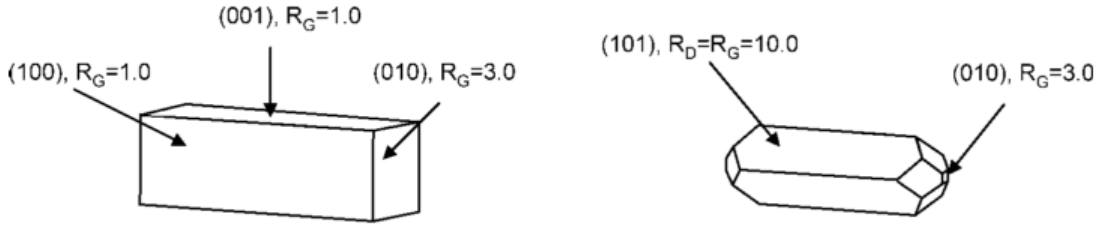

Figure 2-15: Change of crystal habit through temperature cycling if steady-state growth faces are dissolved completely in the dissolution part [3]

The big advantage of this method is, that it uses the existing liquid system, and thus is a non-chemical crystallization route, which manipulates growth and crystal shape only by physical means, by using the crystal's physical properties and without changing the solvent and chemical interactions. [3]

3 Aims of the Experimental Work

The aims of the following practical part of this thesis are

- changing the habit of ASA seed-crystals by
- using a so-called temperature cycling process in a continuously operated tubular crystallizer,
- investigating the influence of different solvents on the crystal habit of ASA crystals (chemical route),
- studying the influence of supersaturation on the crystal habit (non-chemical route) and
- finding a suitable way of detecting the shape-changes preferably in real time.

4 Materials and Methods

The following part will introduce all materials, technical devices and methods that were used for this study.

4.1 Materials

Different solvents and one active pharmaceutical ingredient were studied.

4.1.1 Solute

The solute was the active pharmaceutical ingredient (API) acetylsalicylic acid, short ASA. Its chemical formula is $C_9H_8O_4$. ASA has a density of 1.4 kg/l and a melting point of 140°C. It is slightly soluble in water (about 3 g/l at 20°C) and shows a very good solubility in ethanol (about 165 g/l at 20°C), whereas it is almost insoluble in non-polar solvents, such as alkanes (e.g. n-heptane). Commercial crystals obtained by GL Pharma, type ASS 3020, were studied.

4.1.2 Solvents

For gaining insight into the effect of different solvents onto the cycling-process, the following 7 liquids, shown in Table 4-1, were chosen for first tests.

Table 4-1: Information about used solvents

Solvent	Molecular Formula	Purity	Producer
Ethanol 99.8%	C_2H_6O	≥ 99.8%, denatured with about 1% methyl ethyl ketone	Carl Roth GmbH
Ethanol 96%	C_2H_6O	≥ 96%, denatured with about 1% methyl ethyl ketone	Carl Roth GmbH
Propan-2-ol (Isopropanol)	C_3H_8O	laboratory reagent grade	Fisher Chemical
Acetone	C_3H_6O	analytical reagent grade	Fisher Chemical
1-Hexanol	$C_6H_{14}O$	≥ 98%, for synthesis	Carl Roth GmbH
n-Heptane	C_7H_{16}	≥ 99%, for synthesis	Carl Roth GmbH
Water	H_2O	deionized	

The cycling-solvents were chosen according to their

- Availability

Solvents should not be too expensive.

- Solubility of ASA

It is of big advantage if solubility-data is already available in literature. If not, it needs to be obtained via density-measurements.

- Viscosity

The highest viscosity of a solvent used in this work was about 6 mPas. Since the pressure build-up inside the system was already very high, it is expected to be problematic to crystallize in solvents with a higher dynamic viscosity.

- Density

Densities should be in the range of 0.75 kg/l to 0.9 kg/l at 20°C. If the density is lower, the density difference between ASA-crystals and the solvent leads to sedimentation of the crystals inside the crystallization-tube. This means that the crystals stay inside one part of the tube much longer than desired, at worst until they plug the tube. If the density is higher, it is difficult to create a stable slug-flow.

- Toxicity

Since the setup used in this work is a small lab-setup and neither sealed nor tested for safety, no carcinogenic, mutagenic, reprotoxic (CMR) substances can be chosen. Solvents with preferable low hazard potential were chosen.

- Polarity

In literature it can be read that crystallization of ASA in polar solvents leads to plate-shaped crystals, whereas crystallization in non-polar solvents leads to a more needle-like shape of the product crystals [19], [20].

Table 4-2 shows the boiling temperatures T_S, densities ρ and dynamic viscosities μ of the tested solvents. These are the most important characteristics for the use in the tubular crystallizer, since they determine the temperature range that can be established in the process and the possibility of a stable slug-flow.

Table 4-2: Characteristics of the used solvents

Solvent	**Ts (°C)**	**ρ (kg/l) at 20°C**	**μ (mPas) at 20°C**
Acetone	56	0.790	0.32
EtOH	78	0.789	1.20
1-Hexanol	157	0.820	5.90
n-Heptane	98	0.680	0.41
Isopropanol	82	0.780	2.20
Water	100	0.998	1.00

4.2 Process Equipment

In this section all devices that were used for this work will be presented. To get a general idea of the different parts of this work, the tools are classified into two groups – equipment for cycling experiments and equipment for product analysis.

4.2.1 Equipment for Cycling Experiments

Table 4-3 includes all parts that were required before the crystallization process could be started and that were necessary for the actual cycling process from starting suspension to the final product crystals.

Table 4-3: Equipment for cycling experiments

Device	Model	Manufacturer	Application
Image Analysis	QICPIC/RODOS	Sympatec GmbH, Germany	PSD measurement
Vibratory Sieve Shaker	AS 200	Retsch GmbH, Germany	Sieving of starting material
Focused Beam Reflectance Probe	FBRM® D600R-probe	Mettler Toledo, USA	Suspension stability analysis
Density and Sound Velocity Meter	DSA 5000M	Anton Paar, Austria	Density Measurements
Syringe Pump	Landgraf LA 120	Landgraf Laborsysteme, Germany	Pumping of air
Peristaltic Pump	Reglo Digital MS-2/6V1 13C	Ismatec, Germany	Pumping of seed suspension
Temperature Sensor	Testo 110	Testo AG, Germany	Temperature measurement
Water Bath	Lauda	Lauda-Brinkmann, USA	Heating and cooling

4.2.1.1 Tubing

Tubing is a very important part of a temperature cycling process. For the cycling-tubing two different materials were available:

1. Peroxide-cured silicon tubing
2. PTFE tubing

Both tubes had an inner diameter of 2 mm and an outer diameter of 4 mm.

For the peristaltic pump a special pump-tubing with two or three stops that fit the Reglo pump-cassettes was necessary. Two different types of pump tubing were in use:

1. PharMed BPT (Ismatec, Germany), inner diameter of 1.52 mm
2. Tygon MHSL 2001 (Ismatec, Germany), inner diameter of 1.52 mm

4.2.2 Equipment for Product Analysis

Table 4-4 presents all tools used to characterize the seed and product crystals

Table 4-4: Equipment for product analysis

Device	Model	Manufacturer	Application
Image Analysis System	QICPIC/Lixell	Sympatec GmbH, Germany	At-line product analysis
High Speed Camera	IDT, NX-7-S2	Imaging Solution GmbH	On-line product analysis
Light-Microscope	Leica DM4000 M	Leica Microsystems GmbH, Germany	Off-line product analysis
Scanning Electron Microscope SEM	SEM Ultra 55	Zeiss, Switzerland	Off-line seed and product analysis

4.3 Experimental Methods

This chapter describes which experimental methods came into operation, what the modus operandi of those methods was and which settings were used. No results will be shown here. Results to all methods and experiments will be presented from Chapter 5 on.

4.3.1 Determination of Solubility Curves

The determination of solubility curves of ASA in the solvents, for which no data could be found in literature, was done via density measurements. First a “concentration of ASA vs. density” calibration-curve had to be found at one constant temperature. In this work 40°C were chosen, because all set-temperatures in the cycling processes will stay below this value. Then a saturated solution at a different temperature was prepared, a sample was taken and put into the densitometer, which heated the sample up to the temperature of the calibration curve and measured the density. Since the original temperature of the sample and its density at calibration-temperature were now known, it was possible to find out about the correlating concentration of ASA in this sample by using the calibration factor. . Like this, the first point of the solubility curve (concentration of ASA over temperature) was determined and could be depicted. This procedure was continued at different temperatures until enough points of the solubility curve were determined.

Depending on the slope of the solubility curve and the absolute amount of ASA dissolved to saturate the solvent, the settings for the crystallization process had to be varied.

4.3.2 Preliminary Experiments

In preliminary experiments different solvents were first tested in batch mode. A cooling crystallization with 100 ml of a saturated solvent was carried out at a defined temperature of 22°C. A spatula-tip of seeds was put into the flask containing the saturated solution, then the flask was placed inside a water bath equipped with a cooling thermostat (Lauda alpha RA 12, Lauda, Germany). At the beginning this water bath was at the same temperature as the saturated solution. The flask was stirred with an overhead-agitator. Now the cooling crystallization started by lowering the temperature in 0.5°C-steps every 20 minutes until room temperature was reached. Afterwards, the crystals were filtered and analyzed.

Preliminary cycling experiments were also done. All solvents were saturated, put into the tubular crystallizer and cycled at varying settings to find out about their practicability in a temperature cycling process.

4.3.3 Experimental Setup

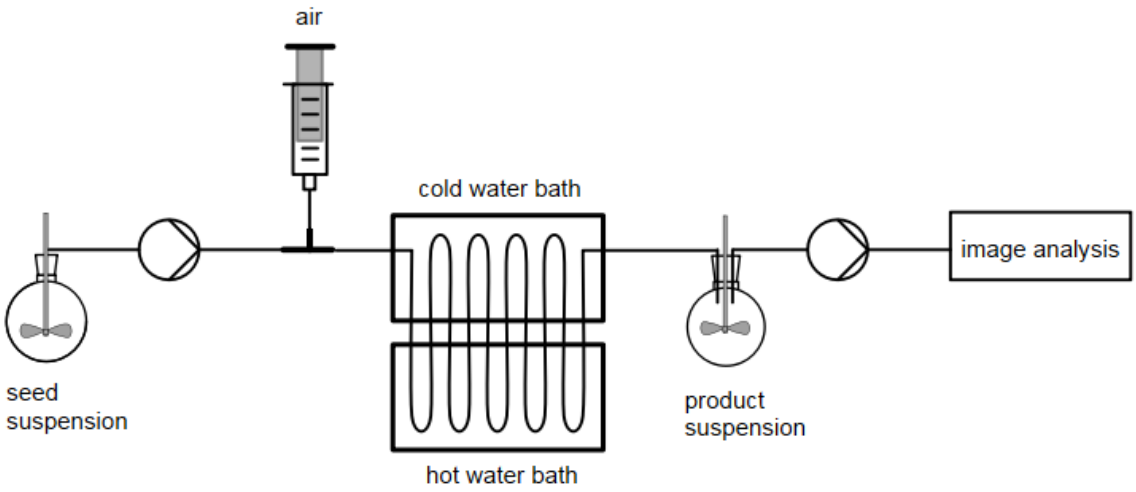

Figure 4-1: Process flow diagram of cycling experiments

The process flow diagram in Figure 4-1 shall give a general overview over the cycling process from seed suspension to analysis of the product crystals. All included steps will be discussed in the following.

The experimental setup for cycling experiments consists of three parts. The first part, shown in Figure 4-2, is located in the hood and contains the starting suspension, which is stirred at constant temperature, the peristaltic pump and two syringe pumps. The peristaltic pump pumps the starting suspension from its vessel into the crystallizer; its set-flow rate is 7 ml/min. The syringe pumps are equipped with two 60 ml syringes each. Both syringe pump tubes are first connected to each other and then to the peristaltic pump tubing via a PTFE T-fitting, which leads into the main cycling-tube. The syringe pumps are required to introduce the air into the suspension flow, which creates the slug-flow. Two syringe pumps are necessary, because they are used alternately to enable a continuous slug-flow. Whenever the syringes of the first pump are empty, it is possible to switch to the second pump, while the syringes of the first pump are refilled with air. The flow-rate of air introduced into the flow is 2.8 ml/min.

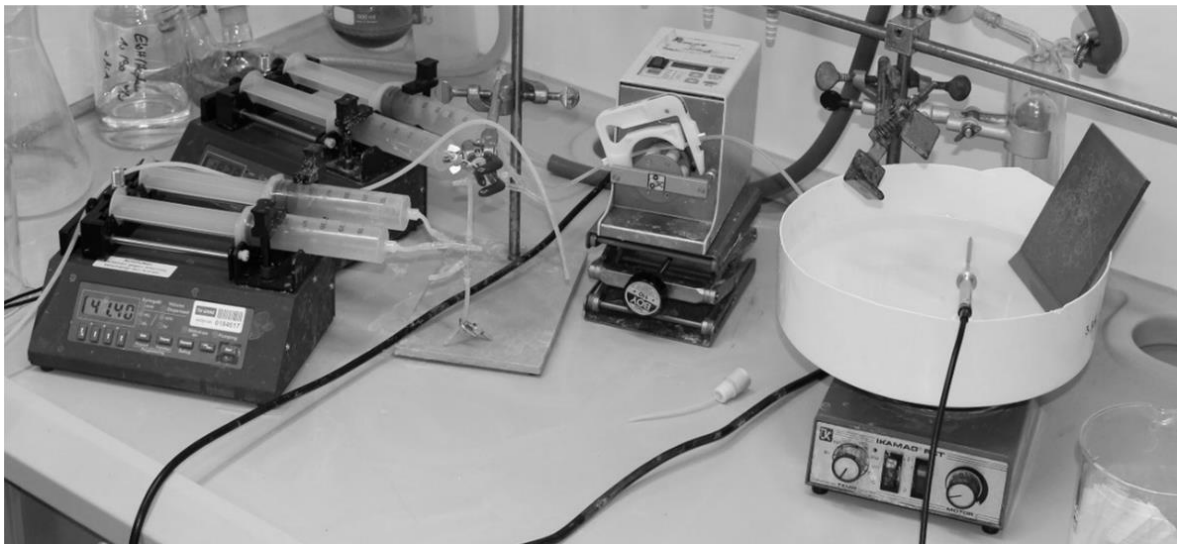

Figure 4-2: Part 1 of the experimental setup

The second part of the cycling-system is shown in Figure 4-3 and consists of the two water baths and the main cycling-tube, a 50 m long tube coiled up alternatingly in the baths. Every cycle of tube has a length of 1.87 m, split 50%:50% to the two water baths. At every changeover from one bath to the other about 15 cm of the tube are located outside the water surrounded by air at room temperature. This leaves about 78.5 cm of tube inside each water bath. The water baths are equipped with a heating coil and an air circulation to ensure equal distribution of the temperature inside the bath. The temperature control of the water bath starts to heat whenever the actual temperature is lower than set-temperature. If the actual temperature is higher than set-temperature, the water baths are cooled with ice. The temperature is checked regularly by eye.

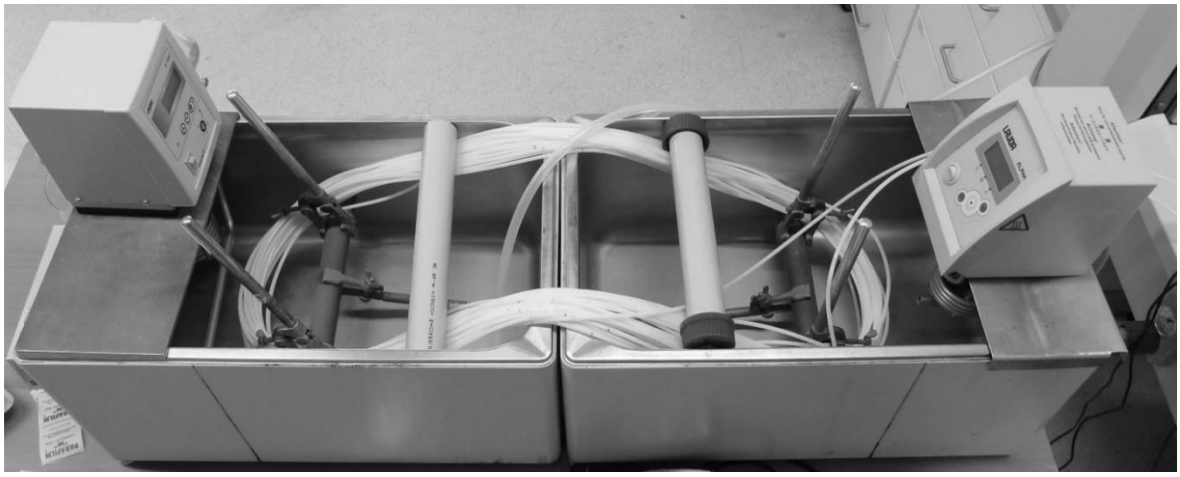

Figure 4-3: Water baths, Part 2 of the experimental setup

The last 50 cm of the main cycling tube carry the product suspension to the third part of the system. Part 2 and 3 are shown in Figure 4-4. The third part of the setup consists of the sampling station, where the product suspension, containing the product crystals, is collected in a 50 ml-round bottom flask and stirred at the same temperature as the starting suspension. Associated with the third part is also the analysis-part, which consists of another peristaltic pump and the image analysis tool QICPIC equipped with the LIXELL-wet dispersion unit. With this setup it is possible to analyze the product crystal suspension at-line, instead of off-line in a microscope. As soon as about 50 ml of product suspension are collected, a measurement is started. The peristaltic pump sucks the product suspension through the cuvette of the QICPIC/LIXELL-combination at about 100 rpm, which equals about 100 ml/min. The dedicated WINDOX 5-software evaluates the pictures of QICPIC's high speed camera and calculates equivalent diameters in order to illustrate the results of this measurement.

A cuvette with 2 mm film-width was chosen, after first tests showed that the 4 mm-cuvette led to an unstable flow pattern in the signal test. The duration of one measurement was set to 20 seconds, a frame rate of 100 Hz was chosen, which sums up to 2000 images per measurement. A few measurements were also conducted with a frame rate of 450 images per second, which is the maximum frame rate.

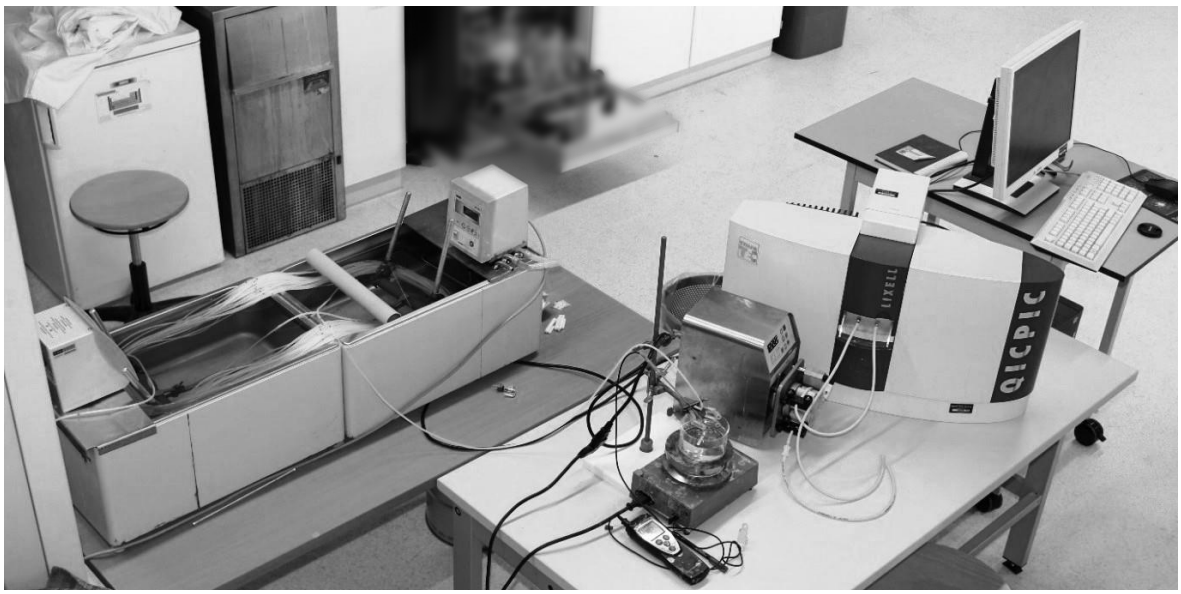

Figure 4-4: Part 2 and 3 of the experimental setup

To get a brief insight how those three parts were arranged, Figure 4-5 shows the whole experimental setup.

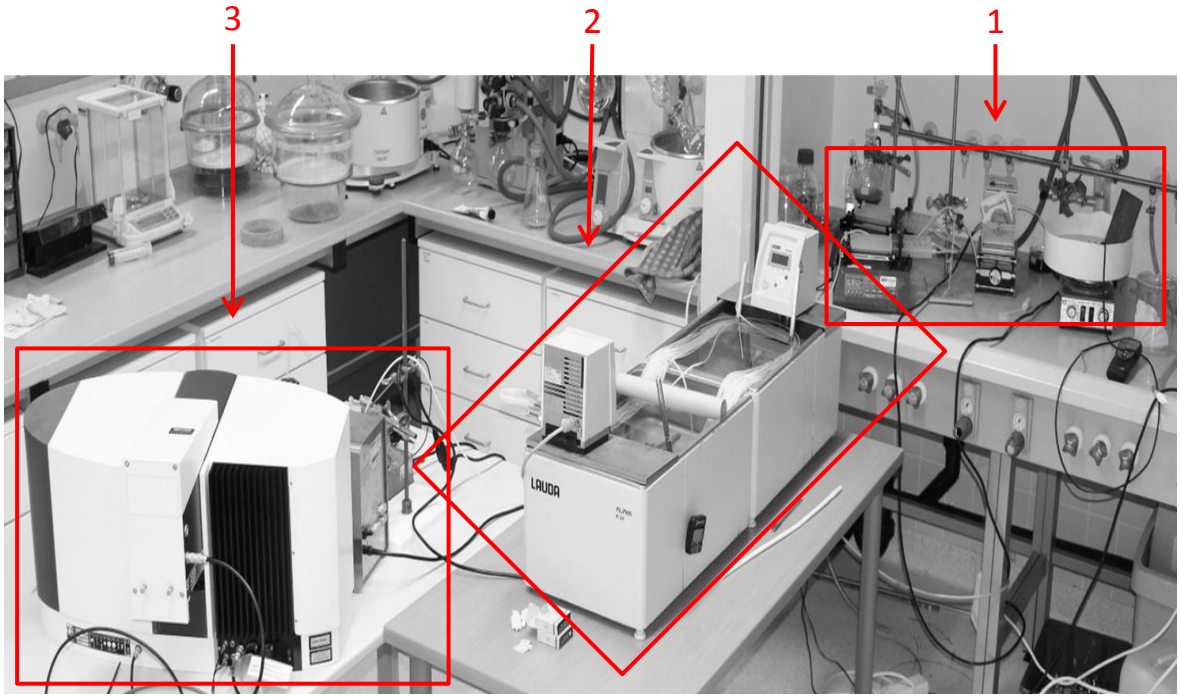

Figure 4-5: Total experimental setup

Tube materials play an important role in the tubular crystallization process. For the peristaltic pump first a PharMed BPT-tubing was used, because it was already available in the laboratory. Later it was found out that this tubing was not suitable for all solvents, so a Tygon MHSL 2001-tubing was purchased. This tubing is designed for aggressive solvents and is plasticizer-free, which means no leaching of unwanted substances from the tube into the liquid. Moreover, the tubing is transparent, which made visual control of the flow inside the pump tubing possible.

For the main cycling tube also two different materials came into operation. The peroxide-cured silicon-tubing is transparent, very flexible, but of limited suitability for solvents. Deposits can be detected easily when keeping an eye on the air bubbles. The PTFE-tubing on the other hand is solvent-resistant, but nontransparent and not flexible. For the main experiments the silicon-tubing was used.

The flow pattern inside the main cycling tube is called slug-flow. Figure 4-6 shows a schematic of a slug flow. Slugs and air bubbles alternate with each other. The crystals used in this work were bigger than in the drawing, only about two to five crystals stayed in each slug. The advantage of this flow pattern is, that aggregation and abrasion can be minimized compared to crystallization in a stirred tank and a very uniform residence time distribution

can be enabled, assuming that each crystal once put into a slug, stays there until the end of the process.

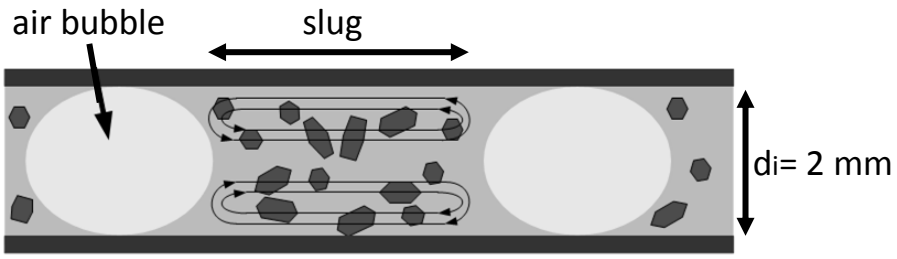

Figure 4-6: Schematic of a slug-flow consisting of air bubbles and flow compartments, called slugs, which contain the crystals [30]

4.3.4 Stability of Seeds

Since the aim of this work was to show that the crystal-shape changes over the cycling process, it is important to show that seed-crystals have a stable shape and size distribution inside the starting solution and thus really change only within the cycling process and not already before. This needs to be confirmed for both the suspension inside the starting flask and the product suspension after running it through the tubular crystallizer kept at constant temperature.

The stability of the size of the seed crystals inside the starting suspension was determined via FBRM-measurements. The FBRM-method works on the principle of laser back-scattering. A laser is emitted from a laser source inside the probe and whenever it hits a particle, it is reflected back into the probe. The time which the beam needs to get reflected, multiplied by the tangential speed of the laser corresponds to the length of the chord which was “traced” by the laser on the particle surface. Depending on the shape of a particle, this chord length can vary significantly from time to time, depending on its position when hit by the laser. A perfect sphere would always have the same chord length, for all other shapes a chord length distribution will be detected. The chord length distribution is not identical to the particle size distribution, but there are approaches to convert the one into the other [31]. The starting suspension was stirred at 22°C and meanwhile monitored with the FBRM probe for one hour.

To prove that the seed-crystals’ habit is stable inside the saturated solution, a cycling experiment was done without temperature difference, at the temperature of the starting suspension. This experiment should yield the same results as for the seeds in the starting suspension itself. Starting suspension was pumped through the cycling system. The solvent

chosen for these tests was EtOH 99.8%. Everything was managed exactly like in the actual experiments, just without any temperature-difference of the water baths. Starting suspension and the hot and cold water baths were constantly kept at 22°C.

To show that the crystal structure was not changed by the cycling process, Raman-measurements were conducted and the spectra were compared. Therefore macro-point (= seven single points) measurements using 30 exposures of 1 second were chosen.

Results of all stability test will be shown in chapter 5.

4.4 Choice of Seeds – Amount and Size

The starting material was sieved in four fractions through a 400, 200 and a 90 µm sieve. In first experiments the fraction of 200 – 400 µm was used as seed crystals. Since the seeds are rod-shaped, this fraction equals crystals of about 200 – 400 µm in their minimum diameter (width of the rod), whereas the maximum diameter (length of the rod) is about 900 µm (= x_{50}). After many tests it was found that these big crystals tend to sediment to the bottom of the tube, ignoring the air bubbles completely by just letting them pass and not moving anymore until they plug the tube. Therefore a smaller fraction of 90 – 200 µm sieve cut size was chosen. Inside the silicon tubing it could be observed, that those smaller seeds follow the flow much better. The amount of sedimenting crystals could be decreased significantly. Figure 4-7 shows microscopy images of the 90-200 µm-seed crystals. According to these images, the seeds have a length of about 450 to 850 µm.

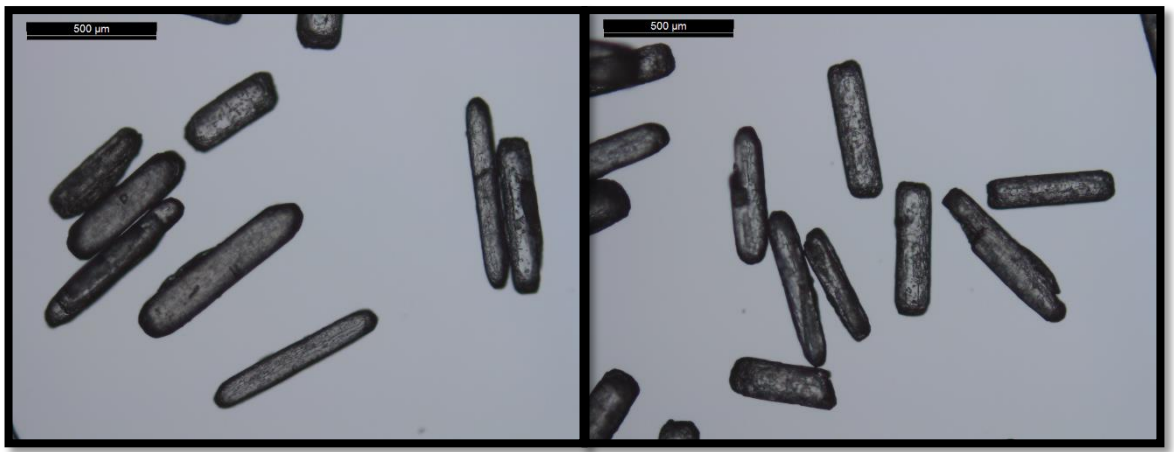

Figure 4-7: Seed crystals 90-200 µm

Not only the size, but also the amount of seed crystals put into the saturated solution plays a big role in achieving comparable results for different solvents. Depending on the slope of

the solubility curve and the absolute amount of ASA dissolvable in each solvent at starting temperature, the amount of seeds was chosen in a way that an equal amount of ASA is available to grow onto the seeds. The amount of seeds compared to the absolute amount of ASA dissolved in the saturated solution was decided to be 1% for all solvents. Bigger amounts from 2% to 5% were also tested, but were found to be too high for solvents with high solubility of ASA, like ethanol.

4.4.1 Temperature Range

In earlier experiments it was found that for ethanol cycling between 17°C and 25°C showed the best results. Many tests were done in order to find a method that does not lead to nucleation and that does not dissolve the seeds completely, i.e. a method that changes the shape of a crystal while keeping the crystals at a comparable size. The temperatures for cycling experiments with all the other solvents were chosen in a way that super- and undersaturation in the water baths are kept constant. The following text explains in detail the calculations and assumptions that were made in order to choose the cycling-temperatures.

4.4.2 Calculation of the Supersaturation

The calculation of the supersaturation is based on the solubility curves of ASA in each of the used solvents. The solubility curve shows the amount of API that is soluble in a solvent at a certain temperature T. This concentration is called saturation concentration c*(T).

The supersaturation S is the ratio of the actual concentration c and the saturation concentration c*.

$$S = \frac{c}{c^*}[-] \tag{1}$$

Since the amount of seeds is very low compared to the amount of ASA that is already dissolved in the solvent (1%), for the calculation it was assumed that growth and dissolution of seeds does not influence the saturation level. From the solubility curves the saturation concentrations over the whole temperature range for each solvent are known. Before entering the first water bath, the supersaturation S is 1, because c= c*. The starting solution is saturated at 22°C starting temperature and also the water bath around it is kept at this

constant temperature. As the process starts, the solution flows into the first, cold water bath. Now S changes.

$$S_{cold\ bath} = \frac{c(22°C)}{c^*\ (T_{cold})} > 1 \qquad (2)$$

The actual concentration c still is the same as in the beginning, but c* is lower than before. At the lower temperature present in water bath 1 (T_{cold}) the solubility decreases and excess solute gets deposited on the crystals, leading to controlled growth. As the state of the suspensions does not exceed the metastable limit unwanted uncontrolled nucleation can be suppressed.

As mentioned above, due to limited residence time in each water bath, saturation equilibrium is not reached. Therefore, also the exact amount of ASA deposited and dissolved during each step is not known. Since the smallest face of an ASA crystal, its (010)-face, is considered stable in both polar and non-polar solvents, it is assumed that the length of a crystal stays the same over the process.

In the hot water bath S changes again, this time in the other direction making the solution be undersaturated.

$$S_{hot\ bath} = \frac{c(22°C)}{c^*\ (T_{hot})} < 1 \qquad (3)$$

Now at T_{hot} the solution is not saturated anymore. ASA seeds that are present in the solution start to get dissolved. In most cases, dissolution happens much faster than growth, therefore, in order not to dissolve the seeds completely, undersaturation has to be adjusted very carefully.

Depending on the solubility curve, each solvent reaches certain set-values of S at different temperatures, but at these temperatures a comparison of the different solvents and their results is possible.

The values that were chosen for S are shown in Table 4-5. The last three rows, marked with a star, were only realized for isopropanol.

Table 4-5: Saturation-Settings for all solvents

Saturation-Setting	$S_{cold\ bath}$ (Supersaturation)	$S_{hot\ bath}$ (Undersaturation)
ΔS_1	1.226	0.888
ΔS_2	1.334	0.864
ΔS_3 *	1.411	0.842
ΔS_4 *	1.474	0.826
ΔS_5 *	1.564	0.811

The values of S for the experiments were set in a way that the characteristic size, the length of the crystals, stayed about the same as for the seeds.

4.4.3 Design of Experiments

After finding the optimal settings and the most suitable solvents in preliminary experiments, the main experiments were designed. The flow-settings, which were experienced to work best, are shown in Table 4-6. At these settings the seeds were transported well by the flow (= flow fast enough) and still had enough time inside each bath to change shape (= flow slow enough).

Table 4-6: Flow rate settings

Pump	Pumped Substance	Flow Rate $F_{v,theor,i}$ (ml/min)
Peristaltic Pump	Seed Suspension	7
Syringe Pump	Air	2 * 1.4 = 2.8

From the chosen flow-rates, the theoretical residence time $t_{res.,theor}$ of each crystal inside the crystallization-system can be calculated. The theoretical flow rate $F_{v,theor}$ (Eq. (4)) is the sum of the flow rates of all pumps, listed in Table 4-6. The total volume that is available inside the tube is the volume of the main crystallization tube $V_{main\ tube}$ plus the volume inside the pump tubing $V_{pump\text{-}tubing}$, which are calculated in Eq. (5) and Eq. (6). $t_{res.,theor}$ is therefore the total volume divided by the theoretical flow rate and equals about 16 minutes, see Eq.(7).

$$F_{v,theor} = \sum F_{v,theor,i} = 7 + 2.8 = 9.8\ \frac{ml}{min} \tag{4}$$

$$V_{main-tube} = = r_{main}^2 * \pi * l_{main} = 0.1^2 * \pi * 5000 = 157\ cm^3 = 157\ ml \quad (5)$$

$$V_{pump-tubing} = \left(\frac{d_{pump}}{2}\right)^2 * \pi * l_{pump} = \left(\frac{0.152}{2}\right)^2 * \pi * 30 = 0.54\ cm^3 = 0.54\ ml \quad (6)$$

$$t_{res.,theor.} = \frac{V_{50m-Tube} + V_{Pump\ Tubing}}{F_{v,theor}} = \frac{157.54}{9.8} = 16.01\ \approx 16\ min \quad (7)$$

The parameters used in the calculations are listed and explained in Table 4-7.

Table 4-7: Parameters used for theoretical residence time calculation

Parameter	Value	Unit	Description
r_{main}=	0.1	cm	inner radius of main cycling tube
l_{main}=	5000	cm	length of main cycling tube
d_{pump}=	0.152	cm	inner diameter of pump tubing
l_{pump}=	30	cm	length of pump tubing

4.4.3.1 Chemical Route Experiments

The chemical route experiments are a comparison of the ΔS_1-cycling-experiments using different solvents. Important for a meaningful comparison is that ΔS is constant and that the amount of seeds divided by the total amount of ASA dissolved in the solvent at the same temperature stays constant.

4.4.3.2 Non-Chemical Route Experiments

The non-chemical route experiments show the influence of temperature cycling on crystal shape for one solvent at different supersaturation-differences. Hereby, a solvent is first cycled at ΔS_1 and right after taking a minimum of three samples, cycled at ΔS_2. In the end, the results of ΔS_1 and ΔS_2 are compared to each other and to the seed-crystal measurements. Of big interest is the magnitude of shape change that can be achieved by a non-chemical route experiment. At best, the magnitude of change would be of about the same order as in the chemical-route experiments, which would make chemical routes redundant and lead to the possibility of shape tuning just by adjusting the supersaturation-difference, i.e. the temperatures.

4.4.3.3 Experimental Test Plan

Table 4-8 shows the settings for the main experiments.

Table 4-8: Settings for main experiments

Solvent	c*(22°C) (g/100g solvent)	ΔS	T_cold water bath (°C)	T_hot water bath (°C)	Amount of seeds (g_Seeds/g_sat. Sol.)	Amount of small seeds/total amount of ASA dissolved
EtOH 99.8%	22.61	ΔS_1	17	25.00	0.00189	1%
		ΔS_2	15	25.70		
Isopropanol	11.59	ΔS_1	19	23.90	0.00107	
		ΔS_2	17.8	24.30		
		ΔS_3	17	24.70		
		ΔS_4	16.4	25.00		
		ΔS_5	15.6	25.30		
1-Hexanol	5.42	ΔS_1	18.60	24.30	0.00053	
		ΔS_2	17.40	24.90		
EtOH 96%	24	ΔS_1	18.20	24.40	0.00200	
		ΔS_2	16.90	24.90		

4.4.4 Analysis

Different methods of analysis were used to find the most suitable one for shape-change detection:

On-line evaluation was possible by using a high speed camera with a frame rate of 500 fps equipped with a 12x zoom lens system (Navitar, USA).

Off-line evaluation of seed- and product-crystals was done with a light microscope. A 5x magnification lens was in use.

Scanning Electron Microscopy (SEM) was used to get information about the surface structure of both the seeds and the EtOH 99.8% product crystals. SEM uses a focused beam of electrons that interact with atoms in the sample. The thereby obtained signals give

information about the sample surface topography. For SEM the samples have to be electrically conductive, at least at the surface. They are therefore usually coated with a very thin coating of electrically conducting material. The ASA-samples were coated with a Gold-Palladium alloy and examined under high vacuum. The energy of the electron beam was 5 kV.

Crystals were also analyzed at-line by the image analysis tool QICPIC equipped with the wet dispersing unit Lixell. All results are based on the evaluation of QICPIC's software Windox 5.

4.4.4.1 QICPIC-Evaluation

To quantify the change of shape over one cycling experiment, it was decided to compare the aspect ratio a of the seed and product crystals. The aspect ratio is defined as the minimum Feret-diameter $d_{Feret,min}$ divided by the maximum Feret-diameter $d_{Feret,max}$.

$$a = \frac{d_{Feret,min}}{d_{Feret,max}} \tag{8}$$

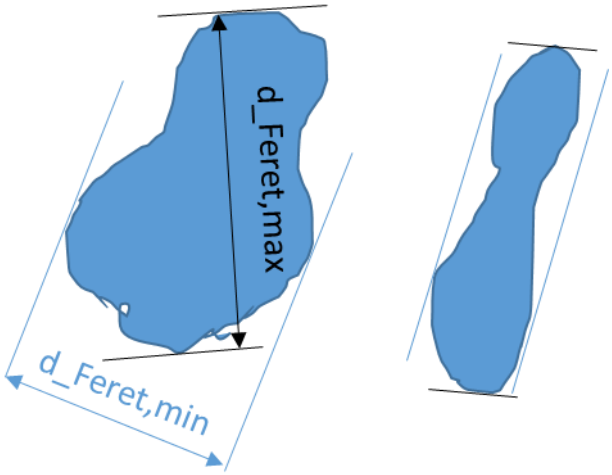

Figure 4-8: Calculating the aspect ratio of particles

Supposing that there are two crystals looking like the ones in Figure 4-8, the aspect ratio of the crystal to the left would be about 0.7, because $d_{Feret,min}$ is not even one third smaller than $d_{Feret,max}$. The crystal to the right however has a $d_{Feret,max}$ of about the same size as the crystal to the left, but its $d_{Feret,min}$ is much smaller. Therefore also its aspect ratio is much smaller, about 0.3. Only a perfect circle has an aspect ratio of 1. The smaller the aspect ratio, the more elongated is the shape of the particle. The aspect ratio gives no information about the

absolute size of a particle. That is why the particle size distribution has to be plotted separately.

The QICPIC camera takes pictures of the crystals, while they are flowing through the cuvette. Since crystals have the freedom to turn within the cuvette, crystals can be observed from different angles. Looking at a rod-shaped crystal from the front and from the side, gives about the same 2D-images and also the calculated aspect ratios will be within the same size-range. Taking images of a plate-shaped crystal will result in very different images. From the front the crystal will look like a plate having a much higher aspect ratio than when looking at it from the side, where it shows a much more elongated shape and may have an aspect ratio as low as the rod-shaped crystal in the example before. Still, the biggest plane of a crystal normally prefers to orient itself parallel to the flow direction, which means that it is most likely to be captured by the QICPIC camera. Therefore, it was assumed that more than half of the images taken by the QICPIC camera show the crystals in a desired position.

4.4.4.2 QICPIC Filter Criteria

It is important to know, that filter criteria have to be used in order to exclude interference factors, for example air bubbles that cannot be totally avoided inside the cuvette. Without filter criteria, the software would count everything that can be detected by the high speed camera, such as dust particles, fibers, air bubbles etc., as a particle. The aim of this evaluation is to set filter criteria in a way that only relevant particles that shall be tracked are counted. On the other hand, the results should not be improved by excluding particles that do not fit to one's wishes, of course. In this work, the diameter of interest is $d_{Feret,max}$. From first measurements of the seed crystals it is known that 80% of the mass of all seeds have a $d_{Feret,max}$ between 420 µm and 850 µm. The smallest 10% and the biggest 10% of the crystals are not included to minimize the risk of evaluating broken crystal parts or big agglomerates. Since the aim of the cycling-experiments is to monitor the shape-change of these seed-crystals and since the temperature range is set in a way that $d_{Feret,max}$ changes only little, the product crystals will have about the same distribution in size. The filter criteria for size is therefore set to $d_{Feret,max} \geq 300$ µm & ≤ 900 µm, after qualitatively checking the QICPIC Particle Gallery, which showed no significant loss of data for this criterion. Aspect Ratio ≤ 0.8 excludes air bubbles independent of their size and sphericity ≥ 0.6 excludes all fibers. Although the term sphericity is normally used for description of 3-dimensional shapes, it is used also for 2-dimensional images in the QICPIC-software.

Figure 4-9 shows measurements of the small seed-crystals plotted without filtering the results (Calc. mode = FERET_MAX) and with the filter criteria mentioned above (Calc. mode = USER_1). For the seeds the curves vary very little, which shows that $d_{Feret,max}$ is a good choice for comparison. The curves only differ for values underneath 400 µm and above 800 µm, which proves that the filter criteria really only exclude big bubbles and small fibres and do not change the outcome of the measurements in the middle part of the distribution, which is the important part for comparison.

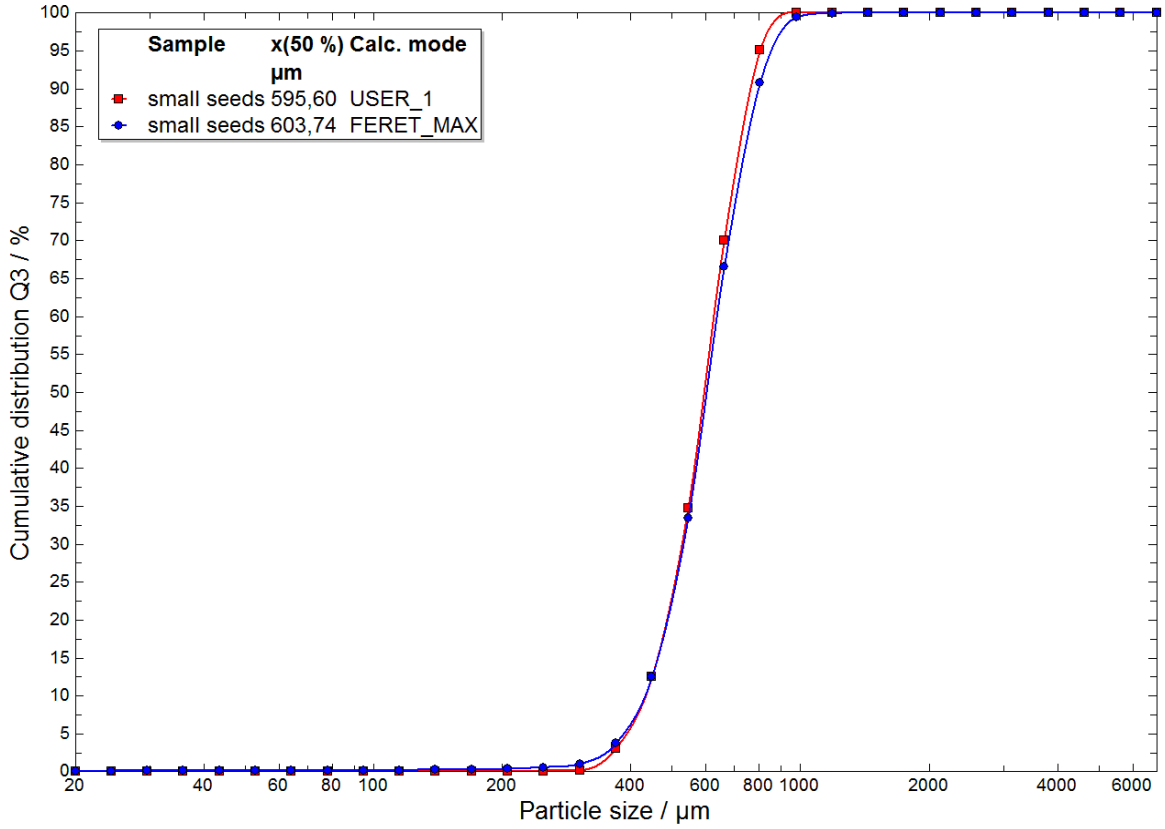

Figure 4-9: PSD of seeds, using the filter conditions in QICPIC versus original data

The aspect ratio distributions of the seeds with and without applied filter criteria, give the same information. In the upper part of Figure 4-10 the curves differ. Without filter criteria, the results move towards bigger values of aspect ratio, because bubbles or big agglomerates are usually rather spherical. Since the comparison in this study shall only include single crystals of a defined size range, it is reasonable to use these criteria and it could be demonstrated that no important information about the crystals is lost.

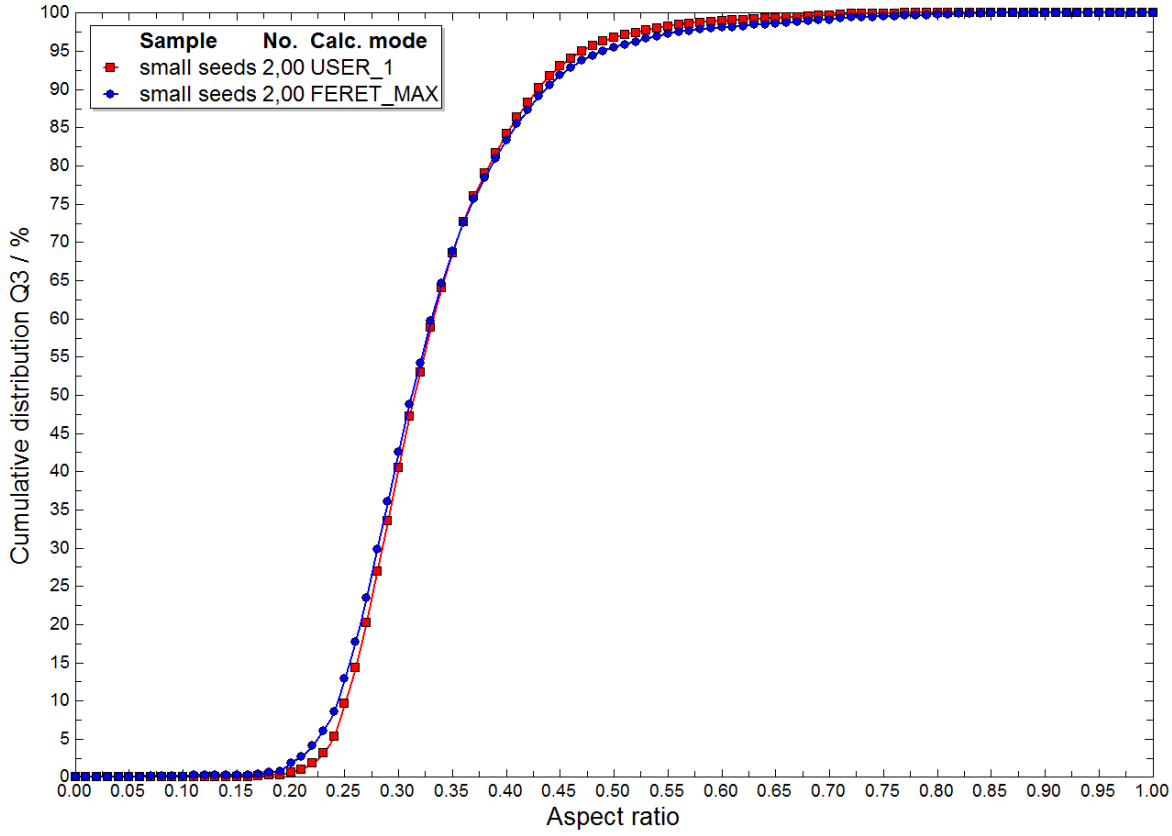

Figure 4-10: Aspect ratio distribution of seeds, filtered versus original data

5 Results & Discussion

5.1 Results of Preliminary Experiments

It was found that the batch test procedure described in chapter 4.3.2 did not work for every solvent. The lower the absolute amount of dissolved ASA and the steeper the solubility curve, the more sensitive to even small temperature changes (<0.5°C) is the solution. It is possible that one solution nucleates right after the first 0.5°C-step, while another one does not nucleate even after 10 0.5°C-steps. Also it is important to know, that due to the big differences in absolute solubility of ASA in the solvents, the amount of seeds given to the solution has to be adapted. Additionally, it was noticed that the cooling thermostat fluctuates too much every time the set-temperature is changed. Usually it reaches a temperature of 0.3°C below the set-point and only then goes up to the actual set-temperature. Since the cooling-steps should be 0.5°C, an additional 0.3°C would make 0.8°C in total, which could again lead to nucleation. Even if no nucleation occurs, it means a variation of 60% in every temperature step and thus ruins the method. Therefore, it was decided that the batch-tests did not provide any information relevant for the actual cycling experiments and that first tests inside the cycling-system should be done instead. The results of those preliminary continuous tests with different solvents are discussed in the following.

5.1.1 EtOH 99.8%

The first continuous cycling-experiments with EtOH 99.8% turned out to work really well. Ethanol's density of 0.789 kg/l and dynamic viscosity of 1.2 mPas seemed to be very suitable for obtaining a stable slug-flow. A solubility curve for ASA in EtOH 99.9% was found in literature [32] and used for experiments in EtOH 99.8%, because the error made hereby is negligible in comparison to the errors that occur because no kinetic data of growth and dissolution are available and therefore all cycling-settings are afflicted with some errors. All solubility curves will be shown after the descriptions of the first tests with different solvents.

Many tests were done in order to optimize the settings for obtaining the best results possible. It was found that when collecting the product solution in a flask, a water bath around it is essential. Without the water bath the temperature inside the flask will not be constant, but vary and thus worsen the product quality by dissolving crystals on their edges, making them seem much more undefined, especially on the borders. The difference can be seen comparing the crystals in Figure 5-1 and Figure 5-2.

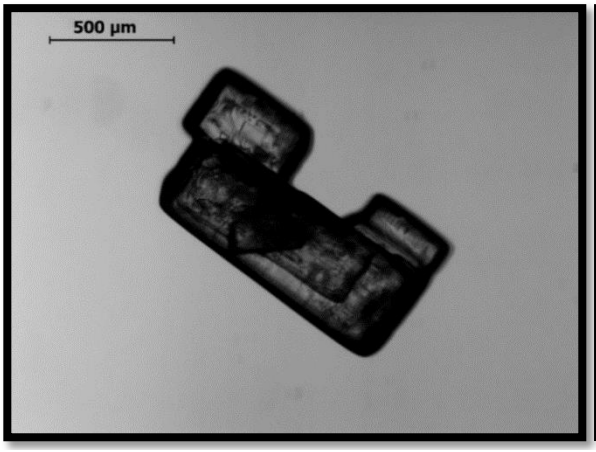

Figure 5-1: Product crystals of EtOH 99.8% from flask without water bath

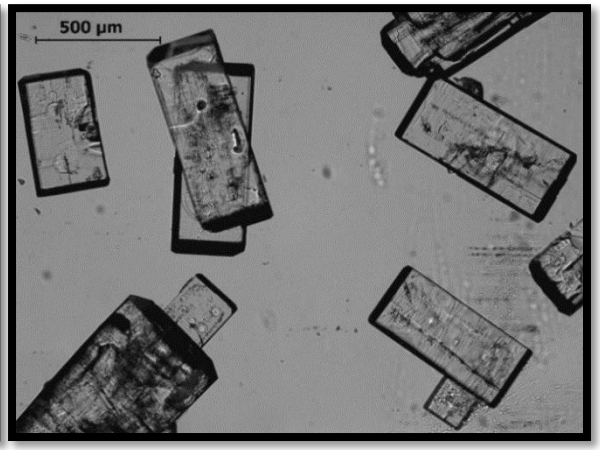

Figure 5-2: Product crystals of EtOH 99.8% from flask kept at constant temperature

5.1.2 EtOH 96%

EtOH 96% was chosen because it was interesting to compare the influence of EtOH 99.8% and EtOH 96% on the crystallization results. The solubility curve for ASA in EtOH 96% was taken from earlier work at our institute and RCPE [30].

Using microscopy no difference to the crystals cycled in EtOH 99.8% could be seen. Therefore, further tests and better product analysis were carried out for EtOH 96% in order to find differences.

5.1.3 Isopropanol

Since EtOH showed good results in first experiments, isopropanol, an alcohol with characteristics similar to EtOH, was tested next. Due to its third carbon-atom, isopropanol is slightly less polar. It was possible to create a stable slug-flow. A solubility curve for ASA in Isopropanol could be found in literature [32]. Figure 5-3 shows some product crystals obtained in first experiments.

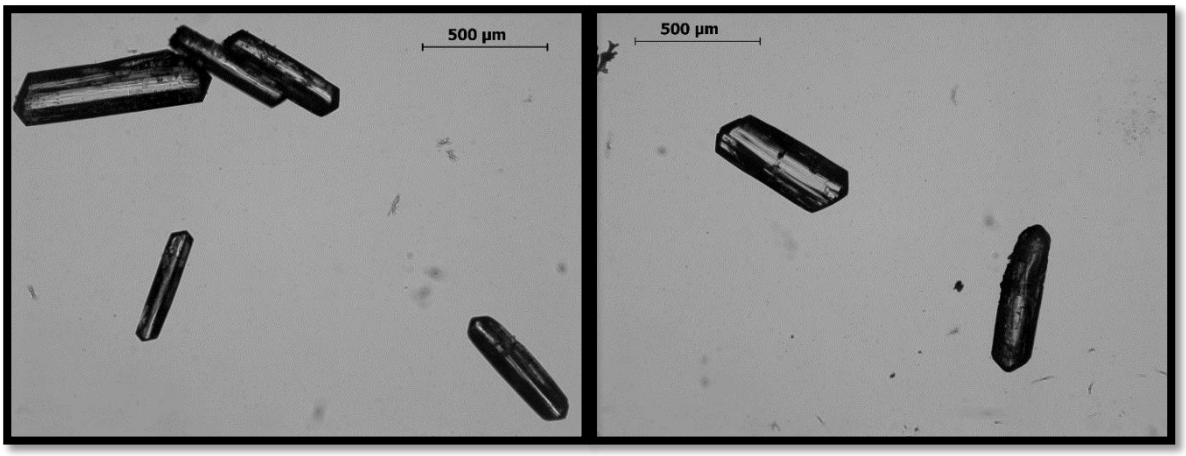

Figure 5-3: Product crystals cycled in isopropanol

5.1.4 Acetone

A solubility curve for ASA in acetone was taken from the same paper as the ones for EtOH 99.8% and isopropanol [32]. Unfortunately, acetone's dynamic viscosity of only 0.32 mPas made processing inside the tubular reactor impossible. No stable slug flow could be created and the seeds did not follow the flow. No product could be obtained and the idea to use acetone for further cycling experiments was dismissed.

5.1.5 Deionized Water

If it is possible to crystallize something from water, it is a big advantage. Deionized water is cheap, absolutely nonhazardous, non-volatile and always available in a laboratory. Solubility data of ASA in deionized water can be found in literature [33]. Theoretically, water would be a great choice – unfortunately not for the tubular crystallizer used in this work. It is almost impossible to create a stable slug-flow, maybe because of water's surface tension and higher density of about 1 kg/l whereas all other solvents have a density in the range of 0.8 kg/l. Therefore, water was excluded from further tests.

5.1.6 1-Hexanol

Since the influence of the polarity on crystal shape was to be studied, it was decided to test another alcohol, one with a longer backbone – 1-hexanol. Its polarity is already much lower than the one of ethanol, but ASA's solubility in it is not as small as in alkanes. Unfortunately, no solubility data of ASA in 1-hexanol is available in literature. The solubility curve had to be determined according to the method described in chapter 4.3.1. The resulting calibration

curve is shown in Figure 5-4, the actual solubility curve is shown in Figure 5-5. Its accuracy was decided to be sufficient, so 1-hexanol was chosen to be part of the main experiments. For this work a linear fit was chosen, in the future a quadratic equation might fit better.

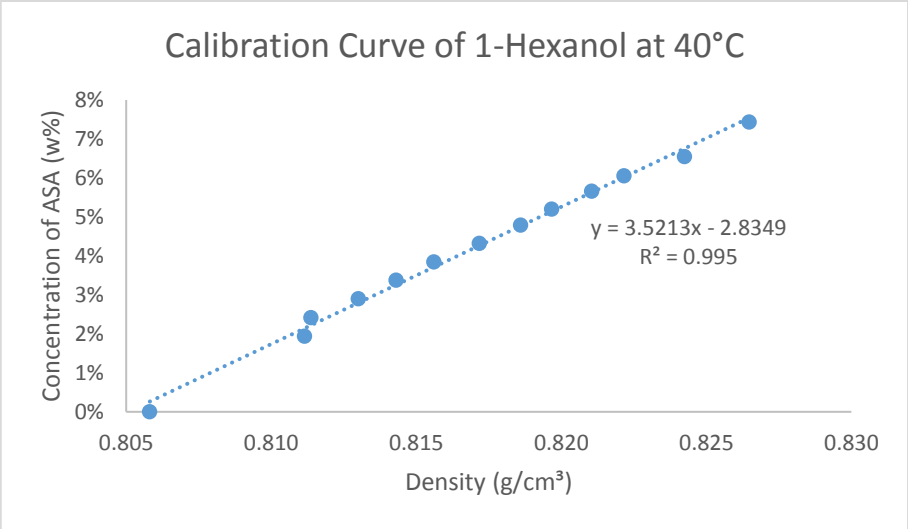

Figure 5-4: Calibration curve of ASA in 1-hexanol

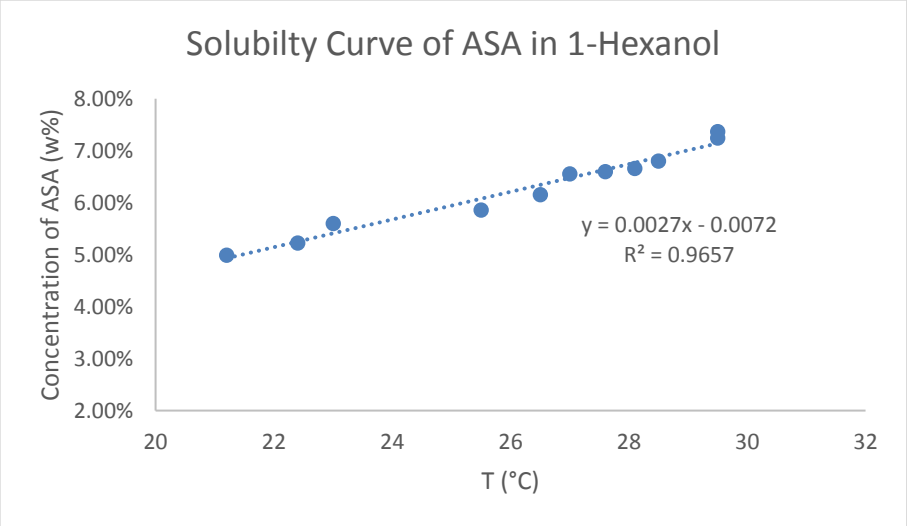

Figure 5-5: Solubility curve of ASA in 1-hexanol

5.1.7 n-Heptane

n-Heptane was the most problematic substance used in this work. It was chosen because of its non-polarity: An alkane without any hydrophilic group seemed to be perfect. In literature many articles report about crystallization of ASA in n-hexane [20]. Since in literature still no sufficient data about the solubility of ASA in n-hexane could be found, it

was decided to use n-heptane, which has characteristics similar to n-hexane, but was not studied much in literature yet.

As a first test, it was tried to saturate n-heptane with ASA in order to roughly assess the range of solubility. It was found that less than 5 g/l were soluble in the pure solvent. Besides, a thin layer of ASA formed covering the whole bottom of the glas flask, making it look like ASA would rather bond with the glass than go into solution with n-heptane. This bad-solubility problem did also arise in literature when working with n-hexane [20]. A possible solution was taking mixtures of n-heptane and EtOH. EtOH increases the solubility of ASA while n-heptane still makes the solution very non-polar. A few tests were done, trying mixtures of EtOH:n-heptane of 90:10 vol%, 80:20 vol%, 70:30 vol% and 50:50 vol%. In microscopy-evaluation of the product-crystals, shown in Figure 5-6, the 70:30 vol%-mixture seemed to give the best results.

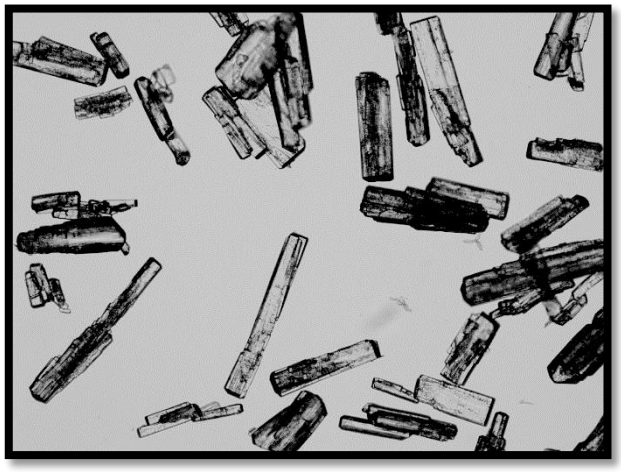

Figure 5-6: Product crystals cycled in a 70:30 vol% EtOH:n-heptane-mixture

Since the solvent-effect on the crystal shape can only be compared if the supersaturation-difference stays constant, the solubility curve of this mixture had to be determined next. The calibration curve was determined and is shown in Figure 5-7.

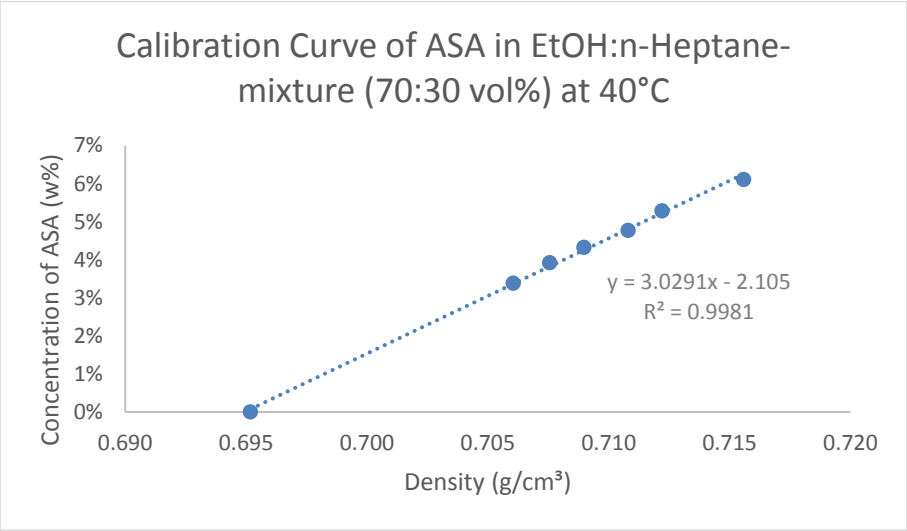

Figure 5-7: Calibration curve of ASA in n-heptane:EtOH-mixture

Obtaining the solubility curve however was more challenging. The data points did not match. Over the whole temperature range, the results from different measurements showed a large variation (see Figure 5-8). From this data no precise calculation of saturation at a certain temperature is possible. Therefore, the unpleasant, toxic mixture was excluded from the solvent-list.

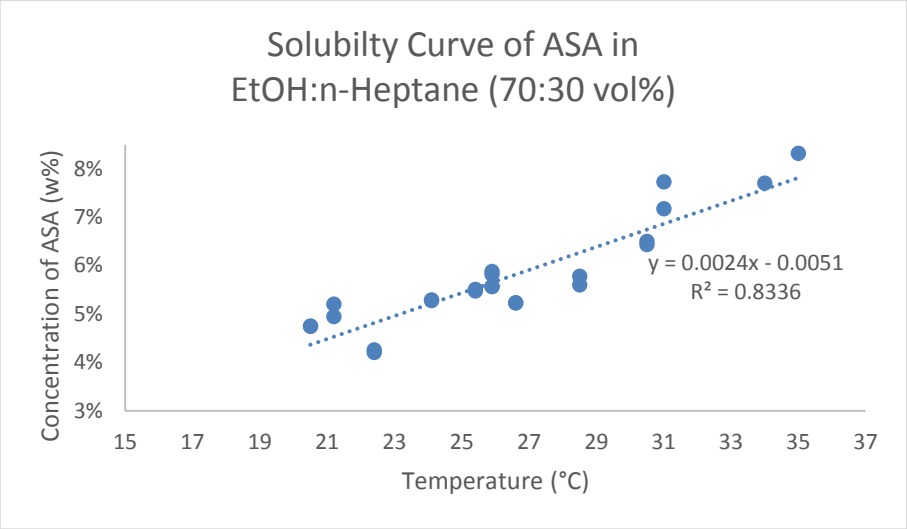

Figure 5-8: Solubility curve of ASA in n-heptane:EtOH-mixture

5.2 Summary of Solubility Data

In Figure 5-9 the solubility curves of all solvents that were chosen for the main experiments are shown. The curves show different slopes and very different values of absolute solubility

of ASA, which makes comparisons of their results in cycling-experiments very interesting. For 1-hexanol and EtOH 99.8% the curves are extrapolated to 15°C.

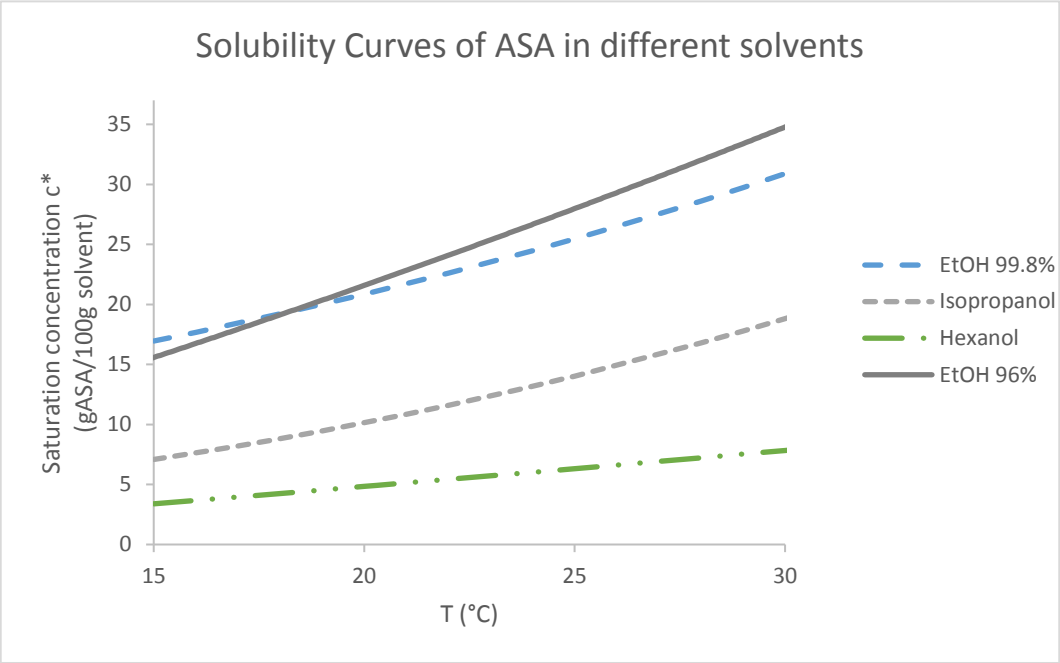

Figure 5-9: Solubility curves of the solvents chosen for the main experiments [32]

5.3 Stability of Seeds

5.3.1 Size and Amount

The FBRM-measurements showed constant values over 60 minutes of testing in all four size classes ranging from 10 µm to 1000 µm. The suspension can therefore be assumed to be stable concerning crystal size and amount. If nucleation took place in the suspension, the counts within the smallest size class would rise significantly. If all crystals grew, counts within the smallest size class would decrease, while the counts within the other three size classes would increase. If the crystals changed their shape, the chord length distribution would change too.

5.3.2 Habit

Figure 5-10 shows the results of the cycling-experiment of the seeds without temperature difference. The diagram shows the averaged curves of 3 to 5 repeated measurements each. The mean values match almost exactly, but the bars indicating the standard deviation within the measurements show that there are deviations of about 30% in the middle section of the

curve representing the cycled crystals. This outcome could have different reasons. Firstly, the stability tests were done with the bigger seed crystals, which already have a larger aspect ratio-deviation than the smaller seed-fraction. The deviation of the seed-measurements is indicated by black bars. Secondly, it could be possible that the starting solution was not yet in equilibrium. Maybe it was filtrated too early and subsequently had to grow onto or dissolve some ASA from the seed-crystals. Still, the averaged results look good and together with the earlier mentioned FBRM-measurements, it can be assumed that the seed-crystals' shape is stable inside a saturated solution.

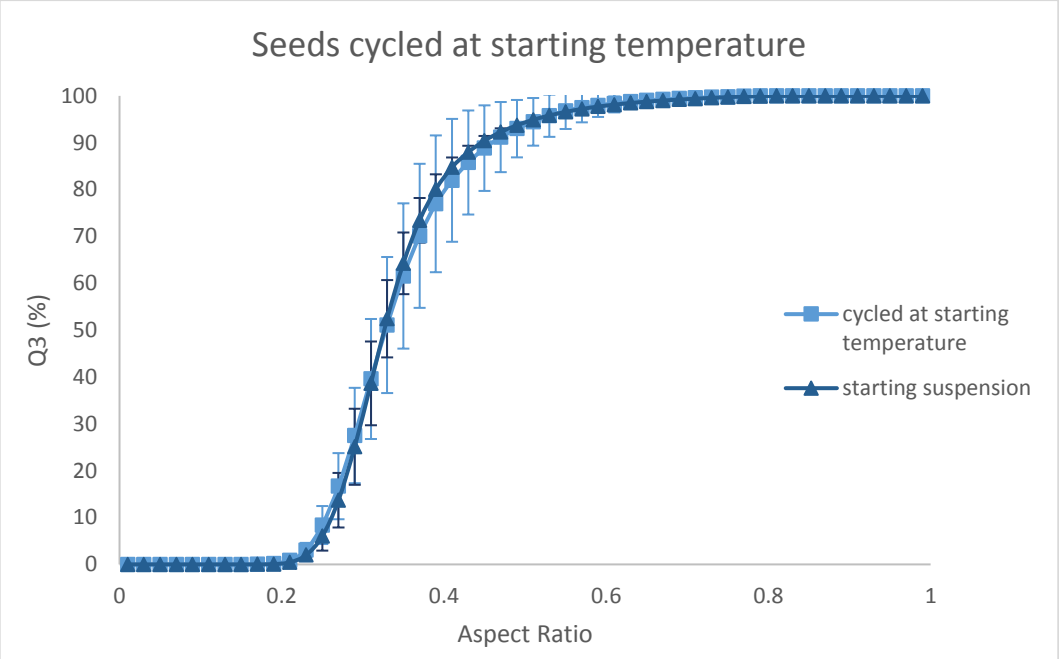

Figure 5-10: Seed-Habit stability

5.3.3 Crystal Structure

Triple Raman-measurements before and after the cycling process led to very similar spectra, shown in Figure 5-11. Only at a Raman shift bigger than 3150 cm^{-1}, the product crystals show another double peak, which is not present in the seed's spectrum. This double peak is very likely to result from the solvent. The characteristic peaks of an ASA spectrum are the ones at 1600 and from 2900 to 3150 cm^{-1}, which look the same in both spectra. It can therefore be reasoned that the crystal structure of both the seeds and the product crystals is the same and no polymorphic change occurs.

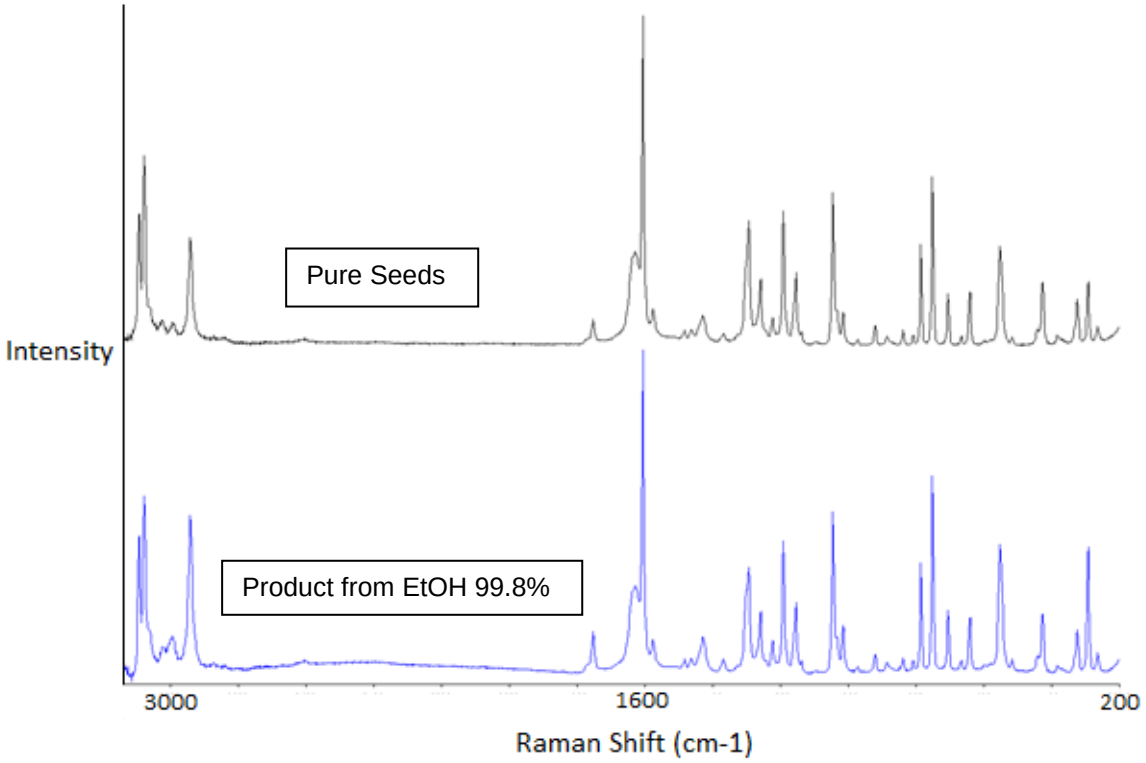

Figure 5-11: Raman-Spectra of seed and product crystals cycled in EtOH 99.8% at ΔS_1

5.4 Residence Time

Tests that measured the time from starting the slug-flow until first crystals and air bubbles appeared at the outlet were done and showed that the actual residence time $t_{res,real}$ differs from the theoretical one. Due to the pressure loss within the system, which is caused mainly by friction between the fluid and the tube-walls, the flow rate of the seed suspension decreases about 20% until the outlet of the tube is reached. Consequently about 5.6 ml/min instead of 7 ml/min of product suspension leave the tube, which leads to a measured flow rate $F_{v,real}$ of 8.4 ml/min and an actual residence time of almost 19 minutes.

$$F_{v,real} = 5.6 + 2.8 = 8.4\ \frac{ml}{min} \tag{9}$$

$$t_{res,real} = \frac{V_{50m-Tube} + V_{Pump\ Tubing}}{F_{v,real}} = \frac{157.54}{8.4} = 18.75\ \approx 19\ min \tag{10}$$

The real residence time is about 17% higher than in theory. Within these 19 minutes inside the process, crystals pass each water bath 25 times, which leads to a residence time of

about 20 seconds per bath. This is the time available for a crystal to dissolve or grow a bit. As soon as the 20 seconds are over, the temperature changes and crystals have to switch to the other extreme, either dissolving or growing.

5.5 High Speed Camera Analysis

In first cycling experiments a high speed camera was used to get a fast insight into how the crystals changed over the process. Exemplary, Figure 5-12 shows how the camera was adjusted and what could be seen in an EtOH 99.8% temperature cycling process. The brighter areas are the inlet and the outlet part of the tube. Air bubbles are the black, flattened objects. Product crystals can be seen in the lower parts of subimage a and b. In subimage b the crystal is especially well-formed and plate-shaped. In subimage a, a rod-shaped seed crystal is visible in the upper part.

Since there was no easy way of evaluating the videos made by the high speed camera and thus, also no possibility of evaluating the shape-change that occurred, this method of analysis was not chosen for the main experiments.

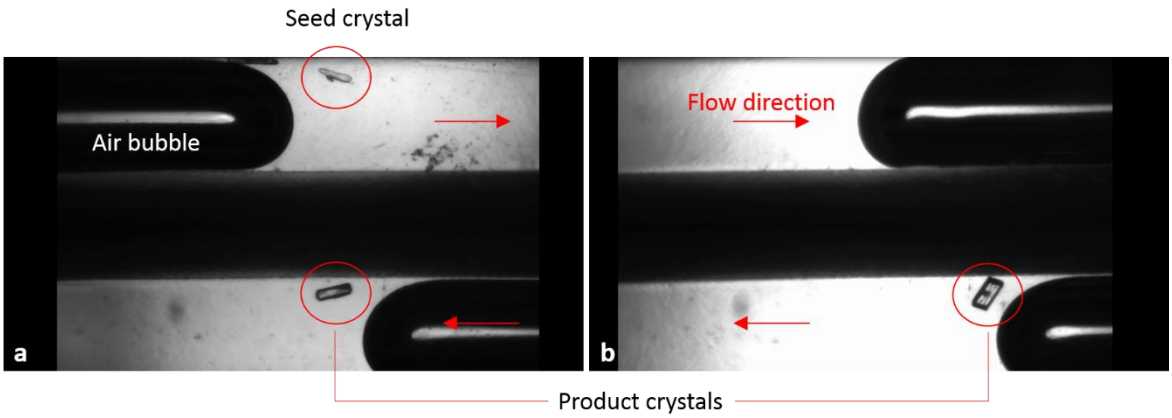

Figure 5-12: High speed camera images of cycling in EtOH 99.8%

5.6 SEM Images

SEM images showed a very different surface topography of seeds and EtOH 99.8% product crystals. While the crystal in Figure 5-13 is very porous and has a rough surface, the crystal in Figure 5-14 has a very smooth surface and sharp edges. This is of big interest for RCPE's further experiments with these samples.

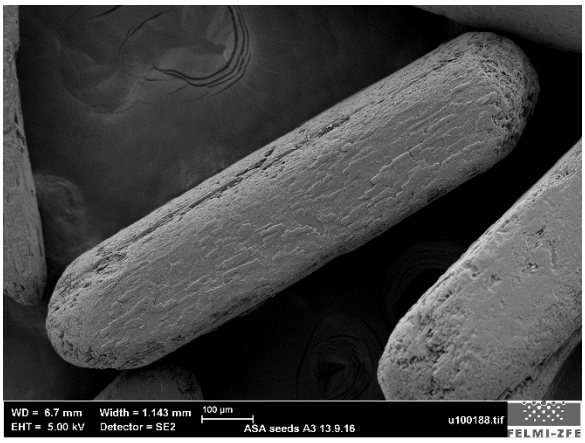

Figure 5-13: SEM-image of pure seeds

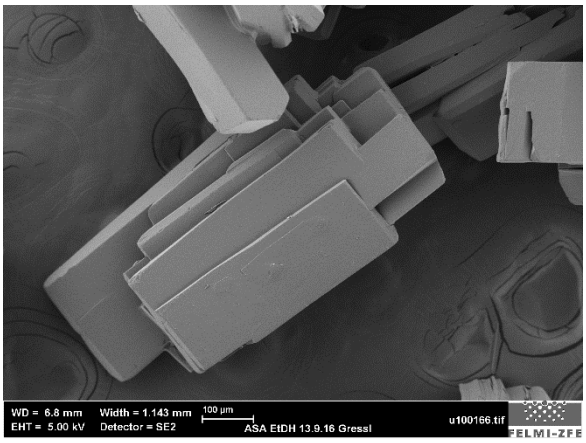

Figure 5-14: SEM-image of EtOH 99.8% product crystals

5.7 Results of the Main Experiments

The main experiments were conducted according to the design of experiments presented in chapter 4.4.3. The analysis method used hereby was the image analysis-option QICPIC/Lixell.

5.7.1 Comparison of Chemical Route Cycling Experiments at ΔS_1

Figure 5-15 shows the resulting curves of the main cycling experiments using the chemical route and Table 5-1 shows their mean aspect ratio values $a_{3,50}$. 50% of the mass of all seeds have an aspect ratio smaller than 0.315. The biggest change to the seeds is achieved when using EtOH 99.8% as a solvent. In this case 50% of the mass of all crystals have an aspect ratio smaller than 0.463 and not even 10% have an aspect ratio smaller than 0.315 anymore. This means, that in the beginning the seeds' length is more than three times larger than their width, whereas after cycling in EtOH 99.8% their length is only twice as large as their width.

Since the equilibrium shape of ASA-crystals is different in every solvent, also the amount of shape change compared to the seed crystal varies. During cycling in EtOH 96% the shape change is smaller, 50% of the mass of all product crystals have an aspect ratio smaller than 0.427.

For isopropanol the shape change over the cycling process is lower than for ethanol, 50% of the mass of the product crystals have an aspect ratio smaller than 0.379. This trend confirms the theory, that crystal shape is dependent on the solvent and its polarity. The

more polar the solvents, the more plate-shaped the product crystals are. The more non-polar the solvent, the more rod-shaped the crystals are.

1-Hexanol is non-polar enough to have an equilibrium shape with an aspect ratio smaller than the seed crystals, $a_{3,50}$ is 0.293.

Since the curves in Figure 5-15 are averages over triple measurements of each solvent, the error bars show the standard deviation of the averaged curves. For a fixed value of aspect ratio, the error bars depict the range of variations in Q_3. As one can see, the error bars do not influence the interpretation of the curves, because they do not overlap. This means that the results using different solvents are significantly different.

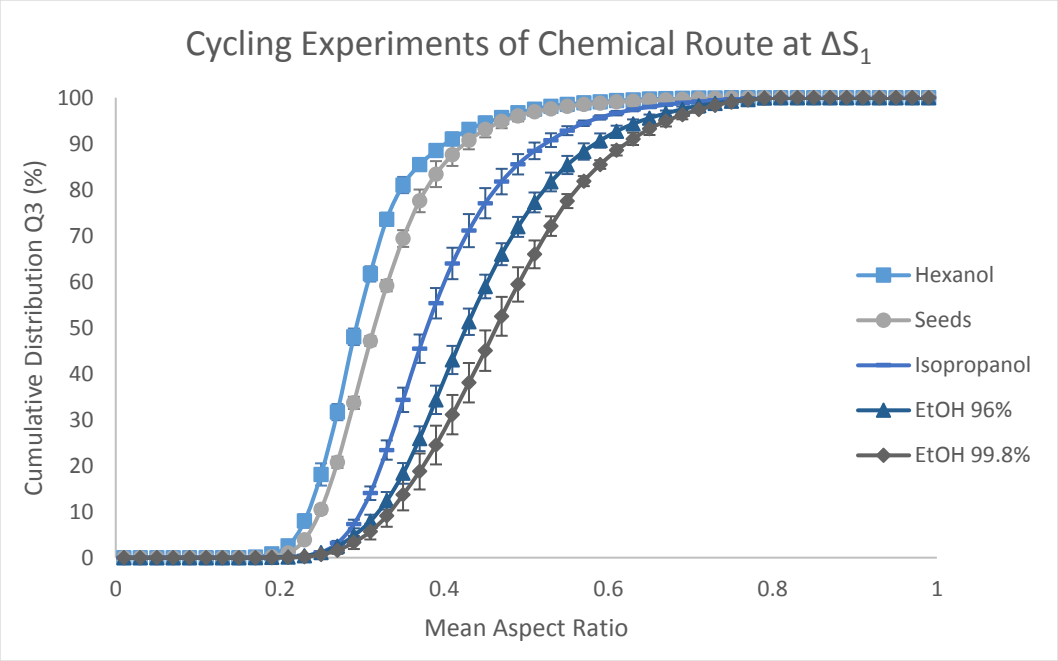

Figure 5-15: Results showing Q_3 over aspect ratio for chemical route ΔS_1-experiments. The error bars show the standard deviation of triple measurements.

Table 5-1 also shows the relative change in mean aspect ratio compared to the seed crystals as a reference for all solvents. While the aspect ratio decreases by 7% when cycled in 1-hexanol, it increases up to 47% when cycled in the other solvents.

Table 5-1: Results of aspect ratio for chemical route ΔS1 experiments

	Mean Aspect Ratio $a_{3,50}$	Relative Change
Hexanol	0.293	- 7%
Seeds	0.315	Reference
Isopropanol	0.379	20.3%
EtOH 96%	0.427	35%
EtOH 99.8%	0.463	47%

It is also possible to interpret the density distributions of aspect ratio for each solvent, shown in Figure 5-16. Because of the different angles, from which the QICPIC camera can take images of the crystals while they are flowing through the cuvette, the peaks in the aspect ratio density distribution become lower and broader the more plate-shaped the product crystals are. Ideally only those images were compared, where the biggest shape change can be seen. In this case, the density distribution peaks should have the same shape as the seed crystals and just be shifted to the right for more plate-like product crystals. Since it is not possible to get only those images, it has to be kept in mind that the actual shape change is bigger than what is shown in the aspect ratio distribution.

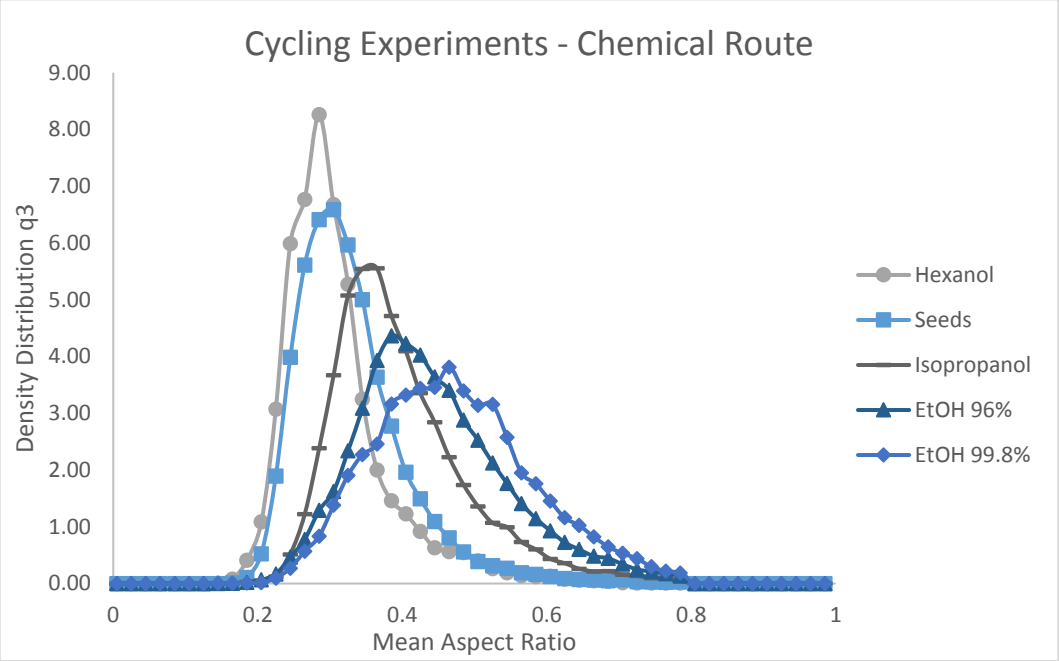

Figure 5-16: Results showing q_3 over aspect ratio, chemical route ΔS_1

The polarity of the solvent definitely influences the exterior shape of an ASA-crystal. The more polar the solvent, the more plate-like the habit of the crystal. As already mentioned, this is in agreement with other studies [19], [20].

Table 5-2 evaluates the sphericity distribution $Q_3(s)$. The sphericity s of a particle is defined as the perimeter of a circle P_C, which has the same projection area as the particle, divided by the actual perimeter of the particle P_{real}.

$$s = \frac{P_C}{P_{real}} \tag{11}$$

The more elongated a particle, the bigger is its perimeter compared to the circle's perimeter. The more rod-shaped a particle, the smaller is its sphericity. Table 5-2 shows a list of the mean sphericities $s_{3,50}$ over three measurements each. This value increases from rod- to plate-shaped exterior, which validates what has been assumed already in the aspect ratio-evaluation. The relative standard deviation in the last column shows really low values below 1.1%, which do not influence the significance of the outcome. The $s_{3,50}$-values are significantly different.

If the sphericity decreased a lot, it could be feared that the crystals agglomerated, which would lead to a very unregular exterior and would also increase the perimeter of this particle, but since $s_{3,50}$ only varies between 0.688 and 0.754 it can be assumed that this change is not due to agglomeration. If crystals agglomerated, their size would change a lot, which is why also the size distribution of the different measurements is evaluated.

Table 5-2: Mean sphericity-values of chemical route ΔS_1 experiments

Sphericity	**Mean Sphericity $s_{3,50}$**	**Rel. Std.-Dev.**
1-Hexanol	0.688	0.3%
Seeds	0.717	0.2%
Isopropanol	0.732	1.1%
EtOH 96%	0.754	0.5%
EtOH 99.8%	0.754	0.9%

The CSDs, shown in Figure 5-17, demonstrate that the crystals' $d_{Feret,max}$ at 50% of the mass-based distribution is about $x_{3,50}$= 600 µm for seeds and product crystals cycled in 1-hexanol. Cycled in isopropanol, EtOH 96% and EtOH 99% the $x_{3,50}$ increases to 650-

690 µm, which equals a maximum difference of 15%. The curves clearly show a trend towards bigger values of $d_{Feret,max}$ for the more plate-shaped crystals in isopropanol and EtOH 96% and 99%, whereas the more rod-shaped crystals of the seeds and the crystals cycled in 1-hexanol are smaller in their $d_{Feret,max}$. This trend makes sense as the $d_{Feret,max}$ of a rod equals about the length of this rod, whereas the $d_{Feret,max}$ of a plate equals the diagonal of the plate-area, which increases the broader a plate and the higher its aspect ratio gets. As already mentioned, the length of the crystals is considered to stay the same in all experiments and also the depth is assumed to vary only little, while the width changes. The particle size measurements and the before presented results fit together well.

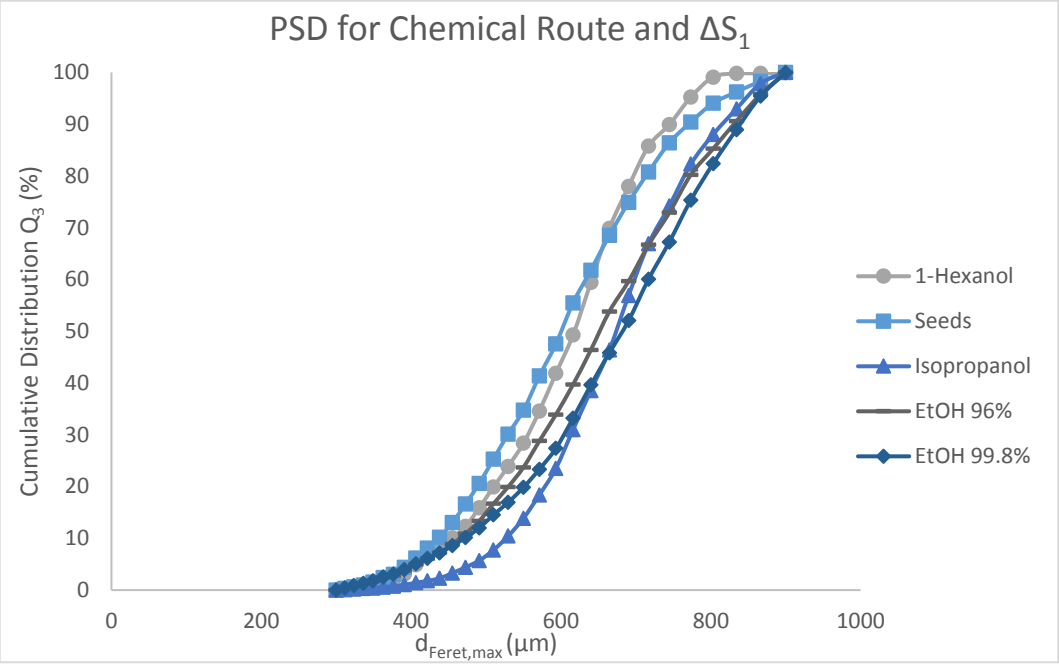

Figure 5-17: CSD after cycling at ΔS_1

Figure 5-18 shows images made by the QICPIC high-speed camera during the flow through the cuvette. Subimage b shows the seed crystals, a the product crystals cycled in 1-hexanol, c the product crystals cycled in isopropanol, d the product crystals cycled in EtOH 96% and e the product crystals cycled in EtOH 99%. It is obvious that the crystals change from a to e. Their length stays rather constant as assumed, whereas their width increases, making the rods in subimage a transform to platelets in subimage e.

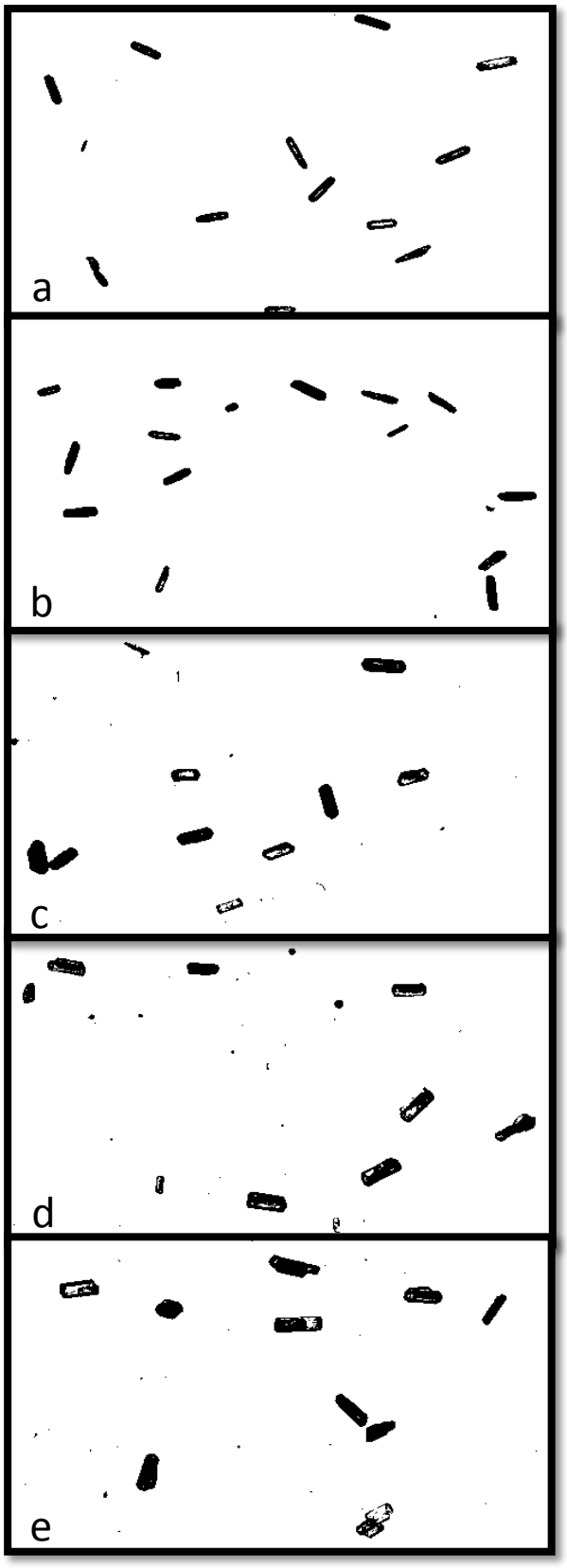

Figure 5-18: QICPIC signal test-images of chemical route ΔS_1 shape-changes; subimage b shows the seed crystals, a the product crystals cycled in 1-hexanol, c the product crystals cycled in isopropanol, d the product crystals cycled in EtOH 96% and e the product crystals cycled in EtOH 99%.

5.7.2 Comparison of Non-Chemical Route Cycling Experiments

The non-chemical route experiments compared different supersaturation-differences ΔS_1 and ΔS_2 for each solvent. The possibility of changing a crystal's shape just by adjusting the supersaturation-difference would be very interesting. One would not have to worry about the right solvent and possible by-products or impurities anymore, but could use the existing liquid system of the previous process and still get the desired crystal shape.

The experiments showed an increase of the effect that was already seen in the ΔS_1-experiment of each solvent. The mean aspect ratio values were evaluated as well as the relative change of aspect ratio compared to the seed crystals. Since the changes obtained in non-chemical route experiments are small, a statistical significance test was carried out to decide, whether the results lead to significant differences. A two-tailed, independent two sample t-test, more precisely a Welch's t-test, was chosen. The Welch's t-test is designed for unequal variances, but keeps the assumption that random errors follow a normal distribution. The null hypothesis (H_0) states that the means of the ΔS_1- and ΔS_2-experiments are actually the same and all differences are purely due to random errors. The alternative hypothesis (H_a) states that the means are significantly different. A confidence level (CL) of 95% was chosen. This means that, in case of rejecting H_0, it is 95% or more sure that this was the right decision, which leaves a maximum of 5% for a wrongly rejection of H_0. These 5% are called significance level or error probability. The calculation was carried out with Microsoft Excel's data analysis add-in, called "Analysis Toolpak". This data analysis tool calculates the probability P that the experimental t-value t_{exp} is bigger or equal to the critical t-value t_{crit} from the t-statistic. t_{exp} is calculated from the amount of samples per measurement, their means and their standard deviations. If P is lower than 0.05 (= 5%), the results are assumed to be significant at the 5% significance level.

Small reminder: ΔS_1-experiments were carried out at a supersaturation of 1.226 and an undersaturation of 0.888, which equals a difference of 0.338. ΔS_2-experiments were carried out at a supersaturation of 1.334 and an undersaturation of 0.864, which is a difference of 0.47 and almost 40% bigger than in the ΔS_1-experiments.

5.7.2.1 Cycling Experiments with EtOH 99.8%

Cycling in EtOH 99.8% led to the biggest change of shape compared to the seed crystals. The values of aspect ratio at Q_3 = 50% can be seen in Table 5-3. The mean aspect ratio $a_{3,50}$ could be raised from 0.315 of the seeds to 0.463 in the ΔS_1-experiments, which equals an increase of almost 47% in aspect ratio. The ΔS_2-experiments led to a mean aspect ratio

$a_{3,50}$ of 0.481, which is an increase of 52.7% compared to the seed's aspect ratio. The cumulative distribution-curves of the experiments are shown in Figure 5-19.

Table 5-3: Averaged results of EtOH 99.8% non-chemical route experiments

EtOH 99.8%	$S_{cold\ bath}$	$S_{hot\ bath}$	Mean Aspect Ratio $a_{3,50}$	Relative Change
Seeds			0.315	Reference
ΔS_1	1.226	0.888	0.463	47%
ΔS_2	1.334	0.864	0.481	52.7%

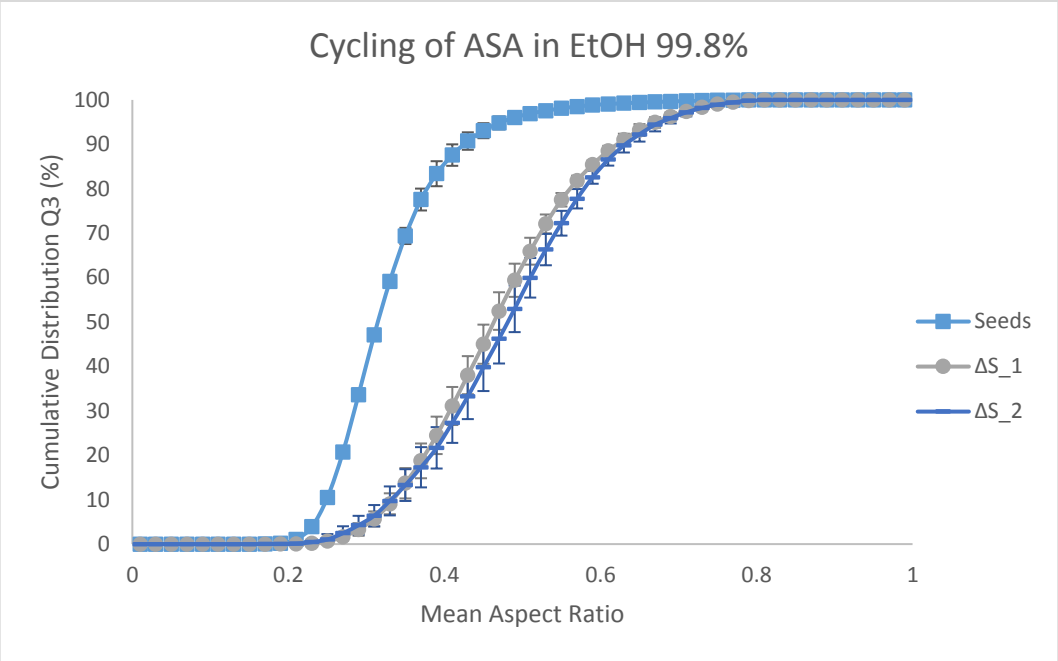

Figure 5-19: Results showing Q3 over aspect ratio, EtOH 99.8%, non-chemical route; error bars show standard deviation of triple measurements

Since the resulting Q_3-curves of the ΔS_1- and ΔS_2-experiments are located very close to each other, it is necessary to do a significance test on the results. Table 5-4 shows an excerpt of the data obtained by the QICPIC measurements. The first column lists values of aspect ratio, from 0.35 to 0.65, which is the range of interest in the EtOH 99%-experiments. The main part of interest ranges always from about Q_3= 10% to Q_3= 90%. The next four columns are dedicated to the means and relative standard deviations of the ΔS_1-and the ΔS_2-experiments. With these values a Welch's t-test was conducted to decide whether the above mentioned null-hypothesis can be rejected. A rejection of H_o leads to a statistically significant difference between the ΔS_1- and the ΔS_2-experiment in one solvent at a CL of 95%. The last column in the table summarizes the outcome of the significance test.

Unfortunately, significant differences are only found at an aspect ratio of 0.55 in this solvent. In ΔS_1-experiments a significantly bigger mass of crystals (about 77.5%) has an aspect ratio lower than 0.55, compared to the ΔS_2-experiments (about 72%). For all other depicted values the differences are not significant. Still, the averaged results of the ΔS_2-experiments show a tendency of intensifying the modification that could already be witnessed in the ΔS_1-experiments.

Table 5-4: Significance of EtOH 99.8% non-chemical route experiments

EtOH 99.8%	ΔS_1		ΔS_2		P	H_0	Significant results?
Aspect Ratio	Q_3 (%)	rel. Std.	Q_3 (%)	rel. Std.	(t_{crit} <= t_{exp})		
0.35	13.7	24.9%	13.3	26.9%	0.873	accepted	No
0.45	45.0	9.8%	39.8	13.4%	0.183	accepted	No
0.55	77.5	2.0%	72.2	3.9%	0.021	rejected	Yes
0.65	93.2	1.4%	92.2	1.8%	0.389	accepted	No

Figure 5-20 shows the density distributions of aspect ratio for all cycling experiments in EtOH 99.8%. Whereas the aspect ratio of the seed crystals varies between 0.2 and 0.6, the product crystals are distributed between 0.2 and 0.8 and the peaks are much lower, which means that the distribution is broader. This outcome verifies the assumption made in chapter 5.7.1, that plates will be photographed either exactly from the side, where they look like rods and have a low aspect ratio, or exactly from the front, looking like the plates that this study aims to see, or from somewhere in between those two extremes. That is, why all values between 0.2 and 0.8 for aspect ratio are present. Still, the peak of the density distribution curve shifts towards higher aspect ratios for ΔS_1 and even more for ΔS_2, which overall confirms that the crystals became more plate-shaped.

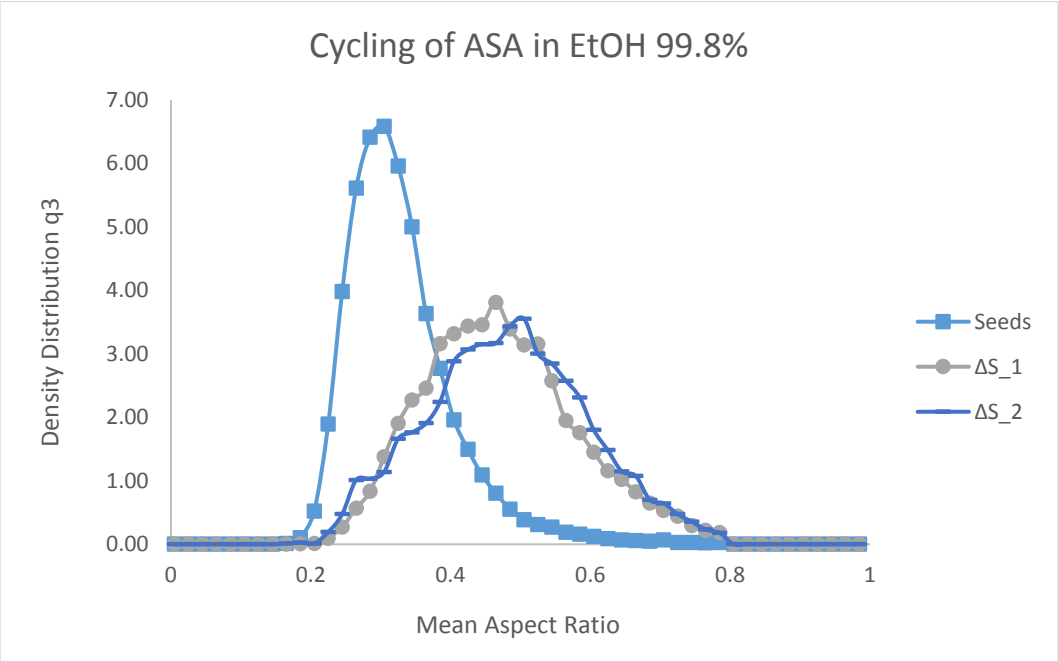

Figure 5-20: Results showing q3 over aspect ratio, EtOH 99.8%, non-chemical route

5.7.2.2 Cycling Experiments with EtOH 96%

The non-chemical route experiments in EtOH 96% led to an increase in aspect ratio $a_{3,50}$ of 35% for ΔS_1, which is a rise from 0.315 of the seeds to 0.427. For ΔS_2 an increase of 40.3% could be reached, equaling an $a_{3,50}$ of 0.442. These values are summarized in Table 5-5.

Table 5-5: Averaged results of EtOH 96% non-chemical route experiments

EtOH 96%	$S_{cold\ bath}$	$S_{hot\ bath}$	Mean Aspect Ratio $a_{3,50}$	Relative Change
Seeds			0.315	Reference
ΔS_1	1.226	0.888	0.427	35%
ΔS_2	1.334	0.864	0.442	40.3%

Figure 5-21 shows the cumulative distributions of the experiments done in EtOH 96%. Compared to the EtOH 99.8%-experiments the crystal's aspect ratio changes less, but the difference between the ΔS_1- and ΔS_2-results seems to be bigger. Looking at Table 5-6, where again the significance of the non-chemical route experiments of ΔS_1 and ΔS_2 and their results is calculated, one can see that the results show a significant difference for aspect ratio-values from 0.45 on. The Q_3-value corresponding to an aspect ratio of 0.45 is 50-60%, which leads to the conclusion that about half of the mass of all particles significantly changes towards a bigger aspect ratio in ΔS_2-experiments compared to ΔS_1-experiments. Still, the results do not show a significant difference over the whole range of aspect ratio.

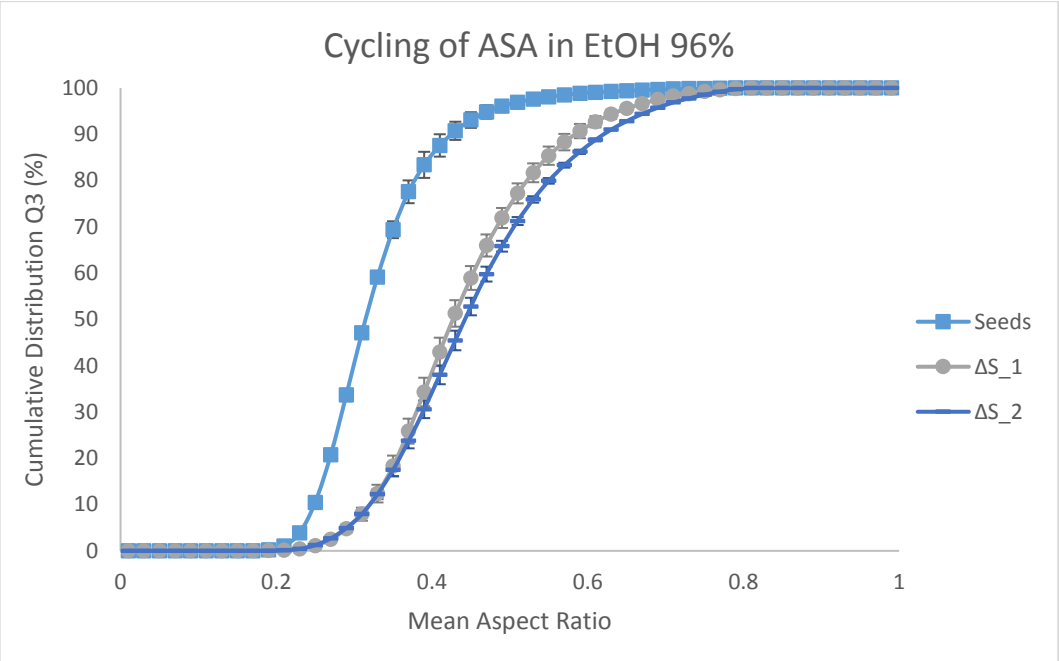

Figure 5-21: Results showing Q3 over aspect ratio, EtOH 96%, non-chemical route; error bars show standard deviation of triple measurements

Table 5-6: Significance of EtOH 96% non-chemical route experiments

EtOH 96%	ΔS_1		ΔS_2		P	H_0	Significant
Aspect Ratio	Q_3 (%)	rel. Std.	Q_3 (%)	rel. Std.	(t_{crit} <= t_{exp})		results?
0.35	18.3	12.3%	17.5	7.6%	0.612	accepted	No
0.45	59.0	4.4%	52.8	3.6%	0.029	rejected	Yes
0.55	85.4	2.3%	79.9	0.8%	0.045	rejected	Yes
0.65	95.6	0.8%	92.8	0.1%	0.025	rejected	Yes

In Figure 5-22 it can also be seen that the cycled crystals' density curves shift to the right towards a more plate-like shape and that the distribution becomes broader, which is the same behavior as for the EtOH 99%-experiments.

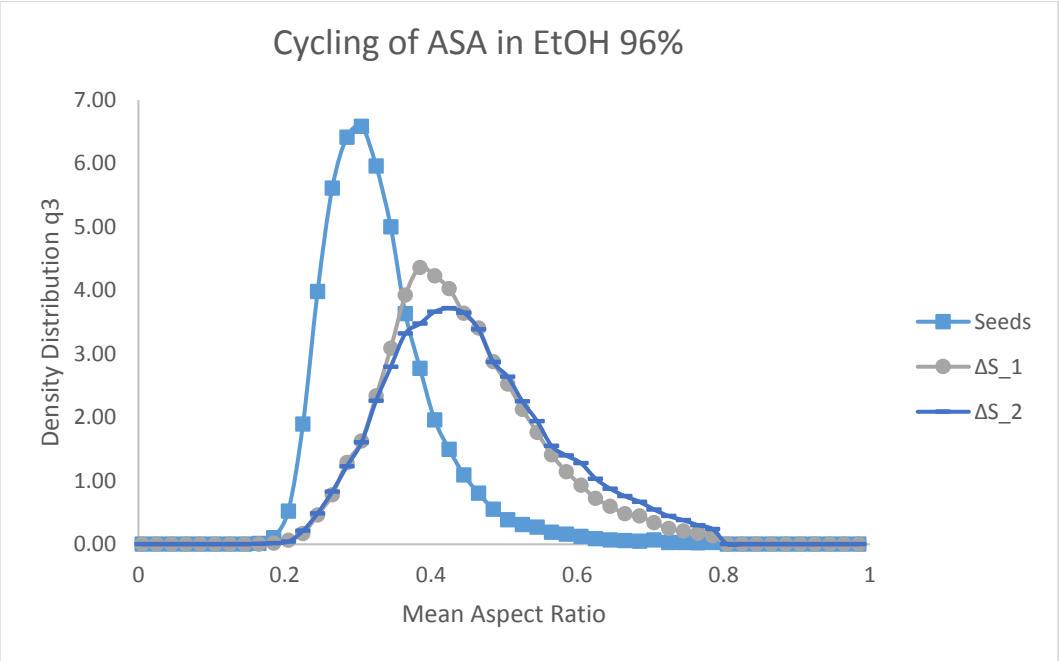

Figure 5-22: Results showing q3 over aspect ratio, EtOH 96%, non-chemical route

5.7.2.3 Cycling Experiments with Isopropanol

Additional experiments were possible when cycling in isopropanol, because the process was especially stable at ΔS_2, where the experiments with other solvents already tended to fail or stop because of plugging or other problems inside the system. Table 5-7 shows the mean aspect ratio values that were reached and their relative change. In the ΔS_1-experiments the aspect ratio change was about 20.3% over the cycling-process, with ΔS_2 about 23.2% compared to the seeds. Curiously, for ΔS_3 the mean change of aspect ratio decreased a bit, and then again rose for ΔS_4 and ΔS_5. In the ΔS_5-experiments 28.9% of change in aspect ratio were achieved.

Table 5-7: Averaged results of isopropanol non-chemical route experiments

Isopropanol	$S_{cold\ bath}$	$S_{hot\ bath}$	Mean Aspect Ratio $a_{3,50}$	Relative Change
Seeds			0.315	Reference
ΔS_1	1.226	0.888	0.379	20.3%
ΔS_2	1.334	0.864	0.388	23.2%
ΔS_3	1.411	0.842	0.381	21%
ΔS_4	1.474	0.826	0.397	26%
ΔS_5	1.564	0.811	0.406	28.9%

The cumulative distributions, shown in Figure 5-23, demonstrate a confusing arrangement of the curves. Even though the curves lie very close to each other, it can be seen, that the ΔS_5-curve is located farthermost right. This confirms the assumption that a bigger supersaturation-difference leads to another increase of the effect already seen in experiments with a smaller supersaturation-difference.

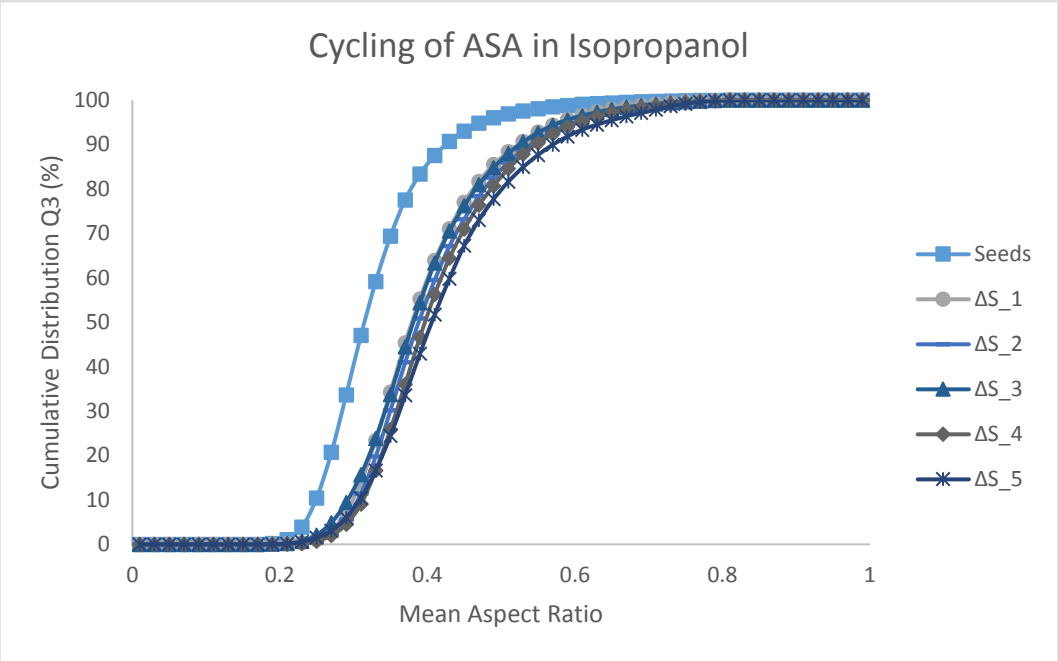

Figure 5-23: Results showing Q3 over aspect ratio, isopropanol, non-chemical route

Separate analysis of the single curves gives again information about the significance of the results. Table 5-8 shows the comparison of the ΔS_1- and ΔS_2-experiments like for the other solvents. Comparing ΔS_1- and ΔS_2-experiments, the results are not significant at all.

Table 5-8: Significance of isopropanol non-chemical route experiments (1)

Isopropanol Aspect Ratio	ΔS_1 Q3 (%)	ΔS_1 rel. Std.	ΔS_2 Q3 (%)	ΔS_2 rel. Std.	P (t_{crit} <= t_{exp})	H_0	Significant results?
0.33	23.4	2.1%	19.8	0.9%	0.071	accepted	No
0.35	34.3	7.7%	30.2	2.6%	0.122	accepted	No
0.45	77.1	4.3%	73.2	1.9%	0.158	accepted	No
0.55	92.8	1.1%	90.9	0.7%	0.063	accepted	No

In Table 5-9 and Figure 5-24 however, the ΔS_1-experiments are compared to the ΔS_5-experiments. Now the results show significantly different results over the whole range of interest. For cycling in isopropanol at ΔS_1 and ΔS_5, the non-chemical route is proven to increase the aspect ratio of ASA-crystals in isopropanol by a mean of almost 29%.

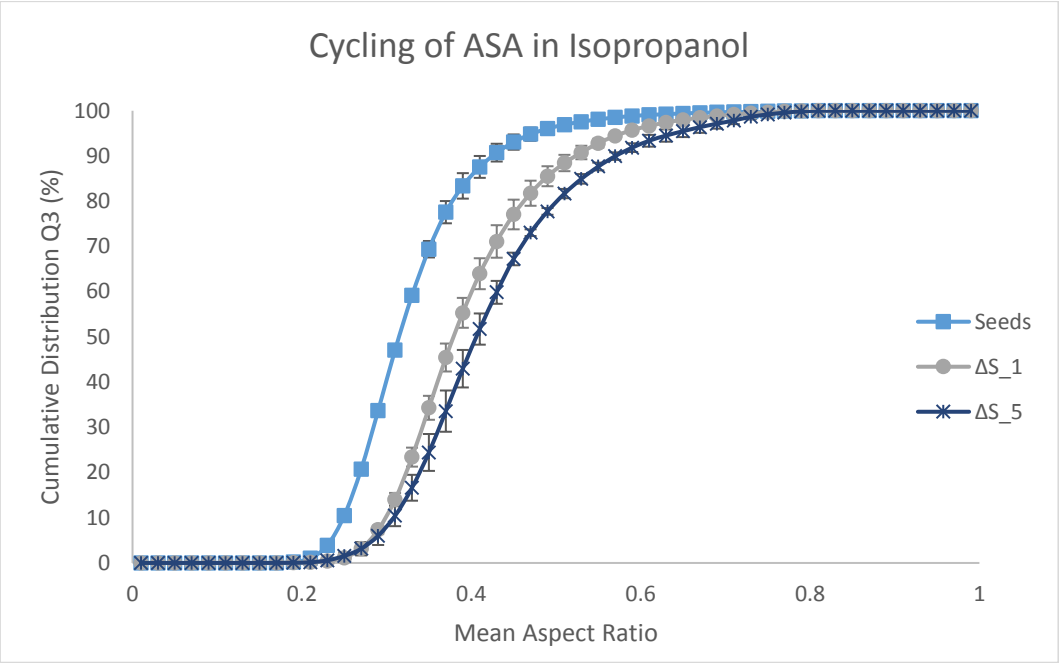

Figure 5-24: Results showing Q3 over aspect ratio, isopropanol, non-chemical route, comparison of ΔS_1- and ΔS_5-experiments; error bars show standard deviation of triple measurements

Table 5-9: Significance of isopropanol non-chemical route experiments (2)

Isopropanol Aspect Ratio	ΔS_1 Q3 (%)	ΔS_1 rel. Std.	ΔS_5 Q3 (%)	ΔS_5 rel. Std.	P (t_{crit} <= t_{exp})	H_0	Significant results?
0.33	23.4	2.1%	16.6	2.9%	0.030	rejected	Yes
0.35	34.3	7.7%	24.4	16.7%	0.039	rejected	Yes
0.45	77.1	4.3%	67.2	2.1%	0.017	rejected	Yes
0.55	92.8	1.1%	87.7	1.0%	0.002	rejected	Yes

This trend can also be found in the density distributions of the results in Figure 5-25. The density distribution of ΔS_1 has the highest peak and is the curve with the smallest aspect ratio. The distribution of ΔS_5 has the lowest peak and is the curve with the highest aspect ratio.

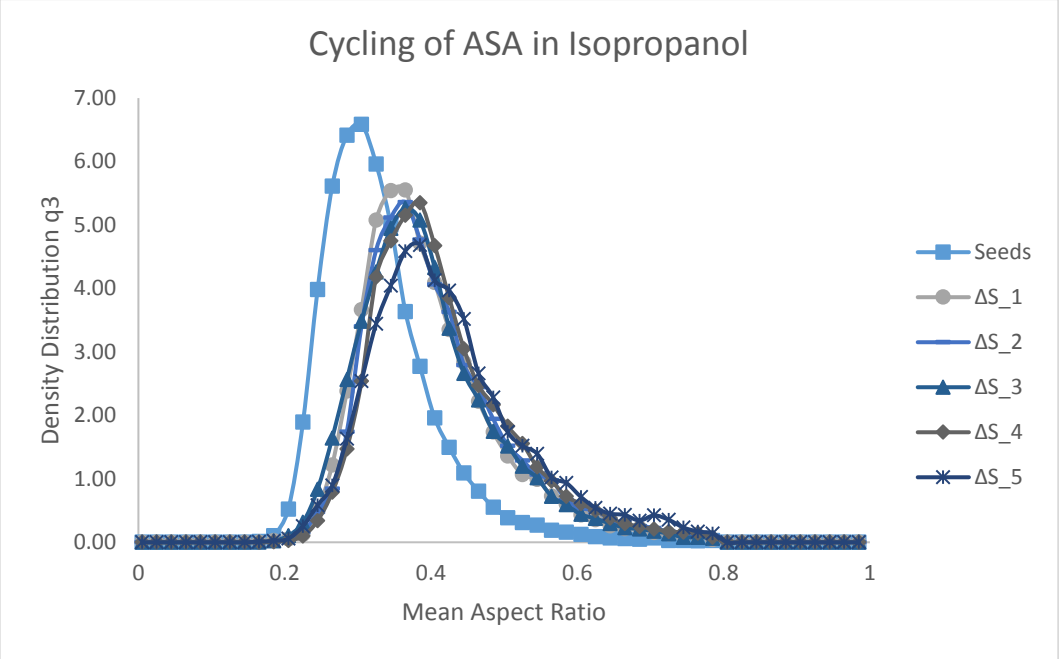

Figure 5-25: Results showing q3 over aspect ratio, isopropanol, non-chemical route

In isopropanol even the highest supersaturation-difference did not influence the flow, which shows that ASA-crystals might grow and dissolve slower in isopropanol than in other solvents.

5.7.2.4 Cycling Experiments with 1-Hexanol

Cycling in 1-hexanol was especially interesting because it led to a change of aspect ratio into the opposite direction, namely it decreased the mean aspect ratio $a_{3,50}$ in the ΔS_1-experiments by 7% and in the ΔS_2-experiments even by 8.9%, as listed in Table 5-10.

Table 5-10: Averaged results of 1-hexanol non-chemical route experiments

1-Hexanol	$S_{cold\ bath}$	$S_{hot\ bath}$	Mean Aspect Ratio $a_{3,50}$	Relative Change
Seeds			0.315	Reference
ΔS_1	1.226	0.888	0.293	- 7%
ΔS_2	1.334	0.864	0.287	- 8.9%

The cumulative distribution curves are shown in Figure 5-26. Unlike before, the curves depicting the results are now located on the left side of the seed-curve. In this illustration the ΔS_1- and ΔS_2-curves look almost identical. In ; error bars show standard deviation of triple measurements

Table 5-11 again the results of the Welch's t-test are shown. H_0 has to be accepted for every value of aspect ratio. Thus, the results cannot be considered significant.

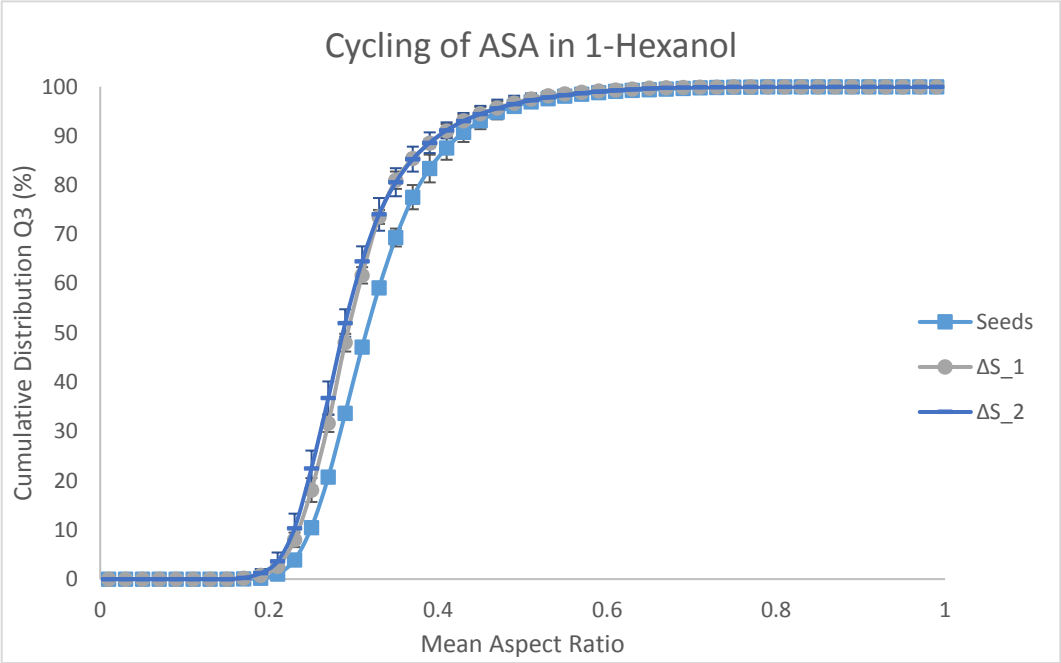

Figure 5-26: Results showing Q3 over aspect ratio, 1-hexanol, non-chemical route; error bars show standard deviation of triple measurements

Table 5-11: Significance of 1-hexanol non-chemical route experiments

1-Hexanol Aspect Ratio	ΔS_1 Q3 (%)	ΔS_1 rel. Std.	ΔS_2 Q3 (%)	ΔS_2 rel. Std.	P (t_{crit} <= t_{exp})	H_0	Significant results?
0.25	18.1	13.4%	22.5	16.1%	0.179	accepted	No
0.29	48.0	3.7%	52.0	5.4%	0.847	accepted	No
0.35	81.0	2.2%	80.6	3.5%	0.966	accepted	No
0.45	94.5	1.5%	94.4	1.8%	0.729	accepted	No

The density distribution curves of the product crystals cycled in 1-hexanol, see Figure 5-27, also show a different behavior than using the other solvents. The peaks of the ΔS_1- and ΔS_2-curves are now higher than the one of the seeds, and the distributions are narrower. Furthermore they are shifted to the left of the seed-curve, which confirms that the product crystals overall have a smaller aspect ratio and thus a more rod-shaped exterior than the seed crystals.

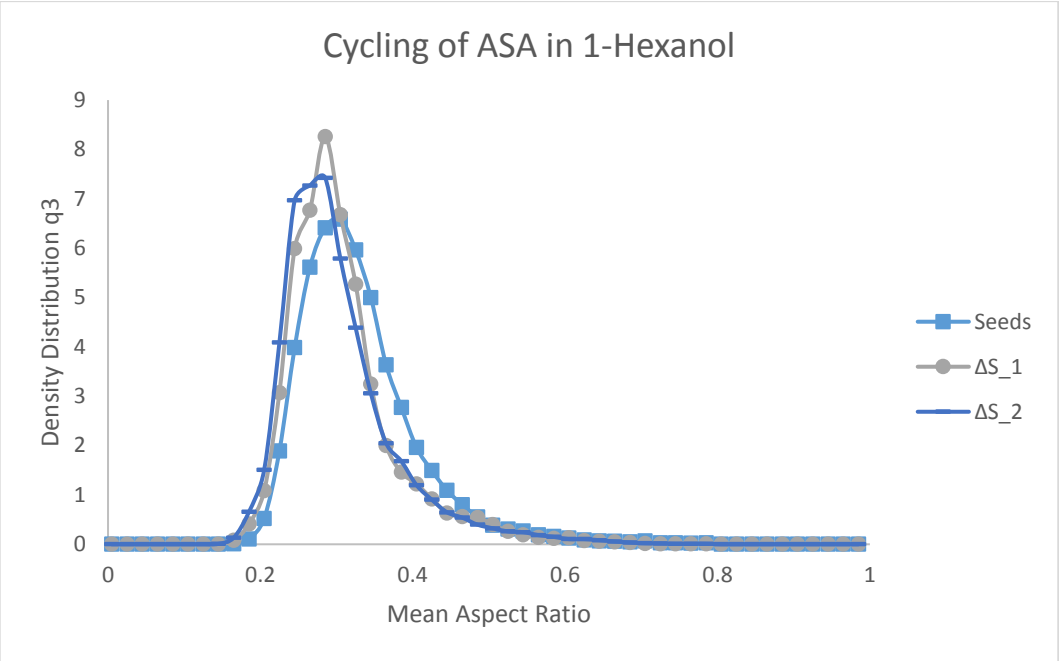

Figure 5-27: Results showing q3 over aspect ratio, 1-hexanol, non-chemical route

5.7.2.5 Findings of Non-Chemical Route Experiments

The main findings of this chapter can be summarized as the following:

- A higher supersaturation-difference increases the shape changes.
- No significant differences were obtained between measurements of ΔS_1 and ΔS_2 according to Welch's t-test.
- Significant differences were obtained only for isopropanol between measurements of ΔS_1 and ΔS_5.

5.8 Discussion

In the following, challenges that appeared during this work, assumptions that proved to be only theoretically true and thoughts about possible improvements will be discussed.

5.8.1 Considerations about Continuous Operation

A truly continuous process includes continuous pre- and post-processing. Otherwise it is only a continuously operated unit operation. In the case of this study, the temperature cycling-process itself is a continuous one, since a second syringe pump was introduced to manage a constant slug-flow. The pre- and post-processing however have to be done batch-wise. The starting solution has to be prepared separately, sample drawing and microscopy-analysis can only be done batch-wise.

On-line analysis via high speed camera-videos is a possibility to monitor the product crystals continuously. The characterization of product crystals via the QICPIC/Lixell-system is managed at-line and can only be done continuously, if the flow rate in the cycling system was the same as in the Lixell-flow cell, which is not the case. The flow cell needs much higher flow rates. Even if the flow velocities were adapted, at least a venting unit would be necessary in between the cycling process and the evaluation, because no air bubbles may get into the cuvette of the flow cell.

5.8.2 ASA Growth and Dissolution Behavior

A correlation between dissolution and growth behavior and supersaturation can be seen when looking at the values in Table 5-12. In ΔS_1-experiments the supersaturation of 1.226 in the cold bath is set to almost 23% above saturation level (S=1), whereas the undersaturation of 0.888 in the hot bath is only about 11% below the saturation level. Since product crystals are about the same size after the cycling process as the seed crystals, it can be concluded that the crystals dissolve about twice as fast as they grow at ΔS_1. For ΔS_2-experiments however, supersaturation of 1.334 in the cold bath is about 33% above saturation-level, whereas undersaturation of 0.864 is not even 14% below saturation level anymore. The bigger the supersaturation-difference, the more pronounced this trend is. The bigger the supersaturation-difference and also the temperature-difference get, the faster the crystals dissolve, but relative to that, their growth is still slower.

Table 5-12: Chosen values for supersaturation-difference

	$S_{cold\ bath}$ (Supersaturation)	$S_{hot\ bath}$ (Undersaturation)
ΔS_1	1.226	0.888
ΔS_2	1.334	0.864

5.8.3 Challenges within this Work

- Calculation of supersaturation

Since no kinetic data of growth and dissolution rates of ASA-crystals in the different solvents were available, the assumptions made for the calculation of S seemed to be the best approximation possible and also worked quite well. For the calculation of S in the water baths, it was assumed that no seeds were present inside the saturated solution. Subsequently, the temperature differences for different solvents were calculated based only on the solubility data of ASA in each solvent. In reality, there are about 1% seed crystals present in the solution. These seeds have an impact on the actual super- and undersaturation achieved in each water bath, depending on the actual growth and dissolution velocities in each solvent. It has to be kept in mind that the error made by the assumptions for the calculation, is not constant for all solvents, but differs depending on the actual velocities of dissolution and growth for each solvent. Another possibility would have been to measure the growth and dissolution kinetics of ASA in each of the solvents.

- Tubing choice

For the main crystallization tubing two materials were tested. The PTFE-tubing is solvent-resistant, but nontransparent and not flexible. The silicon-tubing is transparent and very flexible, but of limited suitability for solvents. The reason, why in the end the less suitable silicon tubing was chosen for the main experiments, was that the experiments worked much better, when the flow pattern inside the tube could be observed. In the current setup it is necessary to see what is happening inside the tube. If seeds start plugging the tube, it can be intervened immediately by knocking onto the tube until the blockage disaggregated. Another problem, air bubbles starting to divide into many small ones, is caused by some deposits that got stuck onto the inner wall of the tube and disturbed their flow. If this is noticed fast enough, it can be counteracted by trying to detach the deposit.

In an optimum process, one should not have to bother about being able to intervene. If the process was automated and stable, the best suited tube-material should be chosen.

- Plugging

In theory, a crystal stays in the same slug from the moment, when it is inserted, until the outlet. In reality, some crystals stay at the very bottom of the tube and let bubbles pass. As long as it cannot be ensured that the seeds stay inside their slug and follow the flow over the whole process, some will remain in the cold bath and will sooner or later inevitably plug the tube, making continuous processing for a pre-defined period of time impossible. To counteract this problem, two things have to be taken care of and brought into balance – the size of the seeds and the density of the saturated solvent. If crystals had the same density as the surrounding liquid, they would not sediment to the ground, they would stay randomly distributed within their slug (low settling velocity according to Stokes law). Since this is not the case and the crystals will commonly show a density difference to the liquid, there is a second way to improve their operation: Adapting gravitational force that is working on them by changing their size. There is evidence that particles that show a very low density difference to the liquid or that are very small in size tend to move with the flow instead of settling [34].

- Filtration

If physical product shall be obtained by collecting the shape-changed crystals or if samples for off-line evaluation shall be taken, a filter is needed. In this study a vacuum pump connected to two frits was used. The product stream was directed into the first frit until the filter material got plugged by the saturated solution. Then the tube-outlet was moved to the second frit. In the meantime the filter paper containing the product crystals was taken out of the first frit, the frit was cleaned with pure solvent and a new filter paper was put inside. Now the tube-outlet was again moved into the freshly arranged first frit and the cleaning procedure could be started for the second frit. In this way it is possible to collect all product crystals, but it is really labor intensive during the filtration process as well as afterwards, when all collected crystals have to be taken off the filter papers and put into a vessel. A possible improvement would be the use of a continuous filtration system like a rotary vacuum-drum filter or some other laboratory-size continuous filtration device.

- Aggregation of crystals

Aggregation leads to a misrepresentation of the results, because all diameters and in the following also sphericity and aspect ratio distributions would be distorted by the divergent values of aggregates. The evaluation filter criteria should exclude agglomerated crystals, but it still has to be kept in mind that some might be counted anyway, if they are small enough or coincidentally shaped in a way that they still fulfill the criteria.

- Stirring

Stirring should be done in a way that the seeds are equally distributed but not mechanically damaged and such, that heat input via agitation does not change the saturation level. Special care has to be taken considering the temperature inside the stirring water baths.

- Varying pressure drop throughout the system

Variation of pressure drop throughout the system happens due to changes of friction inside the tube because of accumulation of deposits, which leads to changes in the actual flow rate and also to variations in the actual residence times of the crystals. Also, the process is very sensitive to height differences. Only 30 cm of upward flow have a big impact on the flow pattern inside the tube. The whole tube should be arranged at the same height, especially the in- and outlet.

5.8.4 Why did Non-Chemical Route Experiments not Achieve Significant Shape Changes?

The objective to reach shape-changes of the order of the chemical route-differences by the non-chemical route could not be achieved. This is mainly due to the small supersaturation-differences. In the current setup it is not possible to achieve higher supersaturation-differences. On the one hand different parameters would have to be determined first, such as the actual velocities of growth and dissolution of ASA in each solvent. On the other hand there are limitations due to the equipment of the tubular crystallizer. A temperature control of ±0.2°C might already be not precise enough and lead to nucleation. Moreover, the main crystallization tube length of 50 meter with an inner diameter of 2 mm already seems to be the maximum possible length with regard to pressure drop problems.

It can be seen for isopropanol and its ΔS_5-experiment, that a bigger supersaturation-difference of 0.75 leads to significant differences, whereas a supersaturation-difference of

0.47 in all ΔS_2-experiments led to insignificant differences. Also, referring to the theory-part of Snyder et al.'s paper, see chapter 2.5.2, it is reported that between 20% and 80% of the crystal in each cycle are dissolved. Since in this study it was not known how much of the crystal is dissolved in each cycle, it is not possible to optimize the residence time in each water bath either, except by trial and error. The new objective should be to find a way of reaching a supersaturation-difference of about 1.5 and compare the influence of supersaturation-settings on the achieved shape change.

5.8.5 Evaluation of Crystal Shape Change via Aspect Ratio

In this work the shape change was evaluated by monitoring the aspect ratio distribution over the process. The aspect ratio was chosen because the change from rods to plates seemed to be described best by it. Of course, aspect ratio only takes into account two dimensions of the crystal. In theory, crystals would have to be evaluated from the same perspective before and after the cycling process, especially if only one face is growing. Since crystals are not always monitored in a fixed position like under the microscope, there is an error within the evaluation. The evaluation does not only take place from a view where a shape change can be seen, but also from other views, which show the crystal from the top or from the side. This is why the aspect ratio density distribution broadens for the product crystals. The presented results therefore show a trend of shape change rather than absolute values.

6 Conclusion and Outlook

In this study it was aimed to change the shape of ASA-crystals by cycles of dissolution and growth. The product crystals were evaluated by an image analysis tool and the shape change was measured by a comparison of the aspect ratio values of seed and product crystals. The experiments were first done by using a chemical route, which means by changing the solvent, then by using a non-chemical route applying different supersaturation-differences.

Being able to influence the exterior of a crystal is of interest in production as well as in handling of particular solids. Industry has a clear desire for optimized material properties, which often are specific to certain crystal faces. This makes research in the field of crystal shape enhancement reasonable and important.

Basis for this study was a paper of Snyder et al., in which they developed a theoretical model for the change of a crystal's habit. They took advantage of the different velocities of growth and dissolution, which most crystal faces have, and showed, that a certain percentage of dissolution of this crystal leads to the disappearance of a certain face, whereas the growing of the crystal afterwards leads to the appearance of either a new face or the particularly fast growth of an already present face.

A tubular plug-flow crystallizer was used for this study, consisting of two water baths, in which the tube is coiled to pass the water baths alternatingly. The experiments led to impressive results for the chemical route of cycling-crystallization. Hereby the solvent used for the cycling process was changed. The experiments were repeated for every solvent using the same seed crystals, the same percentage of seeds with regard to the absolute solubility of ASA in each solvent and the same supersaturation-difference. The supersaturation-difference for each solvent was calculated based on the solubility curves of ASA in the solvent. It could be demonstrated that the aspect ratio of ASA crystals increases with the polarity of the solvent, in which the crystals were cycled. This can be seen in Figure 6-1. The filter criteria for the evaluation were chosen in a way that only single crystals and their change were taken for comparison.

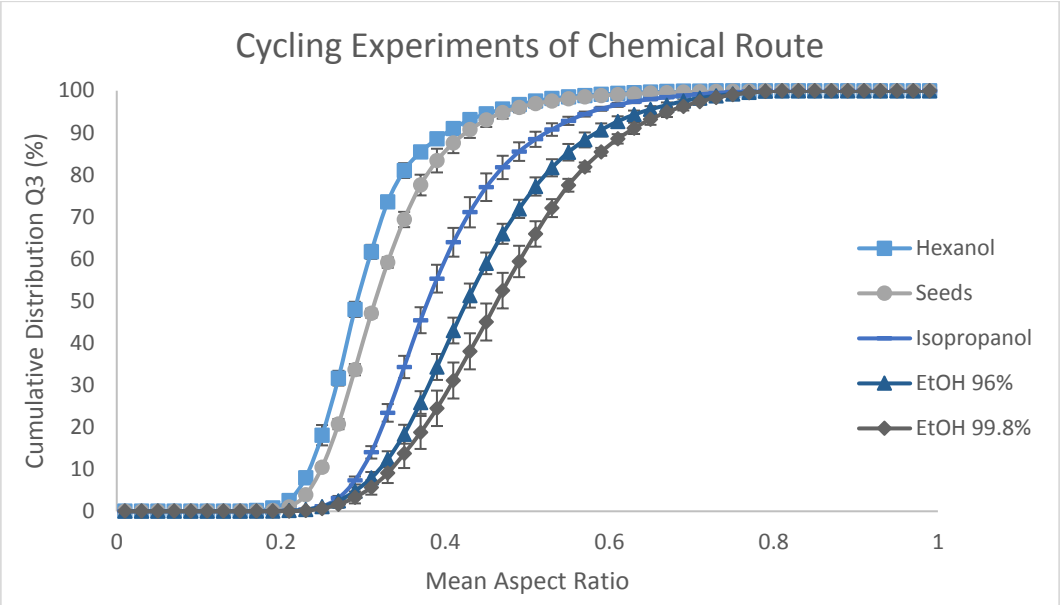

Figure 6-1: Solvent-dependent results; error bars are indicating the standard deviation of triple measurements

The non-chemical route is of big interest, because it uses the present solvent-crystal-suspension and aims at a change of the crystal's shape within this system. The shape change was achieved solely by using different supersaturation-differences. For every solvent, which was already used in the chemical route experiments, the cycling-procedure was repeated at least at one larger supersaturation-difference. It was possible to increase the trend of shape-change, which could already be seen in the chemical route experiments, on average. When conducting a Welch's t-test to decide about the significance of the results, it turned out, that only for isopropanol a significant difference could be achieved over the whole range of interest. This was possible, because a bigger supersaturation-difference could be achieved with this system. The cycling-procedure in isopropanol was particularly stable and a supersaturation-difference ΔS of 0.753 could be reached, whereas the maximum difference for all the other solvents was 0.47. The supersaturation-settings are listed in Table 6-1 and the significantly different results of cycling in isopropanol at ΔS_5 are shown in Figure 6-2.

Table 6-1: Supersaturation-Settings

	$S_{cold\ bath}$	$S_{hot\ bath}$	ΔS
ΔS_1	1.226	0.888	0.338
ΔS_2	1.334	0.864	0.47
ΔS_5 for Isopropanol	1.564	0.811	0.753

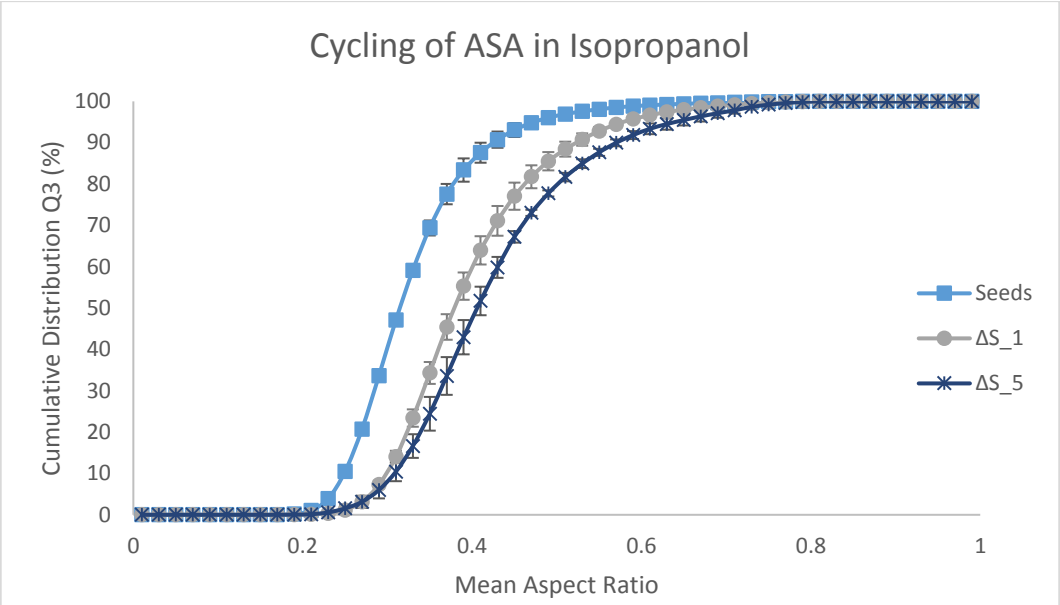

Figure 6-2: Significantly different results for non-chemical route cycling in isopropanol; error bars are indicating the standard deviation of triple measurements

All other non-chemical route experiments did not show significant results over the whole range of interest. The averaged curves though show that the aspect ratio distribution for ΔS_2 shifts to higher values of aspect ratio for EtOH 99.8%, EtOH 96% and isopropanol too. For 1-Hexanol, which is the only solvent that led to a reduction of the aspect ratio over the cycling process, the curve representing the bigger supersaturation-difference shifts to smaller values of aspect ratio, also continuing the first trend.

Although the magnitude of shape change in the non-chemical route experiments is by far not of the same order as in the chemical route experiments, it was still possible to get an insight into the behavior of crystal shape change with increasing supersaturation-difference. The reason, why the non-chemical route experiments did not lead to the desired changes, is that it is not possible to achieve supersaturation-differences high enough to enable this amount of modification.

To enable bigger supersaturation-differences in the future, it would be necessary to know the exact dissolution and growth velocities of ASA in different solvents. Therefore kinetic experiments would have to be conducted. Based on these values, the temperatures could be set much more precisely and it might be possible to run experiments in the current setup.

Bibliography

[1] M. Giulietti and A. Bernardo, “Crystallization by Antisolvent Addition and Cooling,” in *Crystallization - Science and Technology*, M. Andreeta, Ed. 2012, pp. 379–396.

[2] F. Abbona and D. Aquilano, “3. Morphology of Crystals Grown from Solutions,” in *Handbook of Crystal Growth*, G. Dhanaraj, K. Byrappa, V. Prasad, and M. Dudley, Eds. Springer, 2010, pp. 53–92.

[3] R. C. Snyder, S. Studener, and M. F. Doherty, “Manipulation of Crystal Shape by Circles of Growth and Dissolution,” *AIChE J.*, vol. 53, no. 6, pp. 1510–1517, 2007.

[4] J. Chen, B. Sarma, J. M. B. Evans, and A. S. Myerson, “Pharmaceutical crystallization,” *Cryst. Growth Des.*, vol. 11, no. 4, pp. 887–895, 2011.

[5] D. Winn and M. Doherty, “Modeling crystal shapes of organic materials grown from solution,” *AIChE J.*, vol. 46, no. 7, pp. 1348–1367, 2000.

[6] R. C. Snyder and M. F. Doherty, “Faceted Crystal Shape Evolution During Dissolution or Growth,” *Mater. Interfaces Electrochem. Phenom.*, vol. 53, no. 5, pp. 1337–1348, 2007.

[7] G. Yang, N. Kubota, Z. Sha, M. Louhi-Kultanen, and J. Wang, “Crystal shape control by manipulating supersaturation in batch cooling crystallization,” *Cryst. Growth Des.*, vol. 6, no. 12, pp. 2799–2803, 2006.

[8] M. A. Lovette, M. Muratore, and M. F. Doherty, “Crystal Shape Modification through Cycles of Dissolution and Growth: Attainable Regions and Experimental Validation,” *AIChE J.*, vol. 58, no. 5, pp. 1465–1474, 2012.

[9] A. Mersmann, M. Kind, and J. Stichlmair, “Kristallisation,” in *Thermische Verfahrenstechnik - Grundlagen und Methoden*, 2nd ed., Springer, 2005, pp. 413–482.

[10] W. Bogacz and J. Wójcik, “The Metastable Zone of aqueous solutions,” *Chemik*, vol. 68, no. 3, pp. 200–201, 2014.

[11] A. Dévay, “Crystallization,” in *The Theory and Practice of Pharmaceutical Technology*, Pécs: University of Pécs Institute of Pharmaceutical Technology and Biopharmacy, 2013, pp. 255–268.

[12] N. J. Hallas, “THERMOPEDIA™-Crystallizers,” 2011. [Online]. Available: http://thermopedia.com/content/680/. [Accessed: 30-Nov-2016].

[13] J. W. Mullin, *Crystallization*, 4th ed. Oxford: Butterworth-Heinemann, 2001.

[14] N. S. Tavare, “Continuous Crystallizers,” in *Industrial Crystallization - Process Simulation Analysis and Design*, Springer Science+Business Media, 1995, pp. 247–302.

[15] M. Skindzier, K. Kaplan, and A. Roberts, “Crystallizers,” *ENCYCLOPEDIA OF CHEMICAL ENGINEERING EQUIPMENT*, 2014. [Online]. Available: http://encyclopedia.che.engin.umich.edu/Pages/SeparationsChemical/Crystallizers/Crystallizers.html. [Accessed: 02-Dec-2016].

[16] NiTech® Solutions Ltd, “NiTech® Solutions Products,” 2015. [Online]. Available: http://www.nitechsolutions.co.uk/. [Accessed: 17-Feb-2017].

[17] S. Lawton, G. Steele, P. Shering, L. Zhao, I. Laird, and X. W. Ni, “Continuous crystallization of pharmaceuticals using a continuous oscillatory baffled crystallizer,” *Org. Process Res. Dev.*, vol. 13, no. 6, pp. 1357–1363, 2009.

[18] D. P. Woodruff, “How does your crystal grow? A commentary on Burton, Cabrera and Frank (1951) ‘The growth of crystals and the equilibrium structure of their surfaces,’” *Philos. Trans. R. Soc. A Math. Phys. Eng. Sci.*, vol. 373, no. 2039, pp. 20140230–20140230, 2015.

[19] T. Li, B. Li, and M. S. Tomassone, “Surface characterization of aspirin crystal planes using molecular dynamics simulations,” *Chem. Eng. Sci.*, vol. 61, no. 15, pp. 5159–5169, 2006.

[20] L. Cambeiro, J. Jobson, M. Pallay, A. Smith, C. White, and Y. Yermakova, “Crystallization of Aspirin Crystals in Polar and Non Polar Solvents in the Presence of Surfactants : An Experimental Approach to Control Size and Shape of Crystals,” *New Jersey Governor’s Sch. Eng. Technol. Res. J.*, 2006.

[21] A. Danesh, M. C. Davies, S. J. Hinder, C. J. Roberts, S. J. B. Tendler, P. M. Williams, and M. J. Wilkins, “Surface Characterization of Aspirin Crystal Planes by Dynamic Chemical Force Microscopy,” *Anal. Chem.*, vol. 72, no. 15, pp. 3419–3422, 2000.

[22] A. Danesh, S. D. Connell, M. C. Davies, C. J. Roberts, S. J. B. Tendler, P. M. Williams, and M. J. Wilkins, “An in situ dissolution study of aspirin crystal planes (100) and (001) by atomic force microscopy,” *Pharm. Res.*, vol. 18, no. 3, pp. 299–303, 2001.

[23] P. M. Vishweshwar J.A. Oliveira, M. Peterson, M.L. Zaworotko, M.J., “The Predictably Elusive Form II of Aspirin,” *J. Am. Chem. Soc.*, vol. 127, no. 14, pp. 16802–16803, 2005.

[24] A. D. Bond, R. Boese, and G. R. Desiraju, “On the polymorphism of aspirin,” *Angew. Chemie - Int. Ed.*, vol. 46, no. 4, pp. 615–617, 2007.

[25] A. D. Bond, R. Boese, and G. R. Desiraju, “On the polymorphism of aspirin: Crystalline aspirin as intergrowths of two ‘polymorphic’ domains,” *Angew. Chemie - Int. Ed.*, vol. 46, no. 4, pp. 618–622, 2007.

[26] A. D. Bond, K. A. Solanko, S. Parsons, S. Redder, and R. Boese, “Single crystals of aspirin form II: crystallisation and stability,” *CrystEngComm*, vol. 13, no. 2, p. 399, 2011.

[27] T. R. Welberry, E. J. Chan, D. J. Goossens, and A. P. Heerdegen, “Diffuse scattering as an aid to the understanding of polymorphism in pharmaceuticals,” *Metall. Mater. Trans. A Phys. Metall. Mater. Sci.*, vol. 43, no. 5, pp. 1434–1444, 2012.

[28] A. Harrison, R. Ibberson, G. Robb, G. Whittaker, C. Wilson, and D. Youngson, “In situ neutron diffraction studies of single crystals and powders during microwave irradiation,” *Faraday Discuss.*, vol. 122, pp. 363–379, 2002.

[29] K. Adhikari, K. M. Flurchick, and L. Valenzano, “Effects of volumetric expansion in molecular crystals: A quantum mechanical investigation on aspirin and paracetamol most stable polymorphs,” *Chem. Phys. Lett.*, vol. 621, no. February, pp. 109–116, 2015.

[30] M. O. Besenhard, R. Hohl, A. Hodzic, R. J. P. Eder, and J. G. Khinast, “Modeling a seeded continuous crystallizer for the production of active pharmaceutical ingredients,” *Cryst. Res. Technol.*, vol. 49, no. 2–3, pp. 92–108, Mar. 2014.

[31] A. V. Pandit and V. V. Ranade, “Chord Length Distribution to Particle Size Distribution,” *AIChE J.*, vol. 62, no. 12, pp. 4215–4228, 2016.

[32] G. D. Maia and M. Giulietti, “Solubility of acetylsalicylic acid in ethanol, acetone, propylene glycol, and 2-propanol,” *J. Chem. Eng. Data*, vol. 53, no. 1, pp. 256–258, 2008.

[33] A. Apelblat and E. Manzurola, “Solubilities of L-aspartic , DL-aspartic , DL-glutamic , p-hydroxybenzoic , o -anistic , p -anisic, and itaconic acids in water from T= 278 K to T =345 K,” *J. Chem. Thermodyn.*, vol. 29, pp. 1527–1533, 1997.

[34] T.-C. Hung, R. H. Piedrahita, and A. Cheer, “Bio-inspired particle separator design based on the food retention mechanism by suspension-feeding fish.,” *Bioinspir. Biomim.*, vol. 7, no. 4, pp. 1–12, 2012.

Table of Figures

Figure 2-1: Different ways of reaching supersaturation zone from stable state (A): through isothermal evaporation (B), through cooling (C) or through cooling and evaporation (D) [11] 3

Figure 2-2: Information flow-diagram of a continuous MSMPR crystallizer [13] 6

Figure 2-3: FC crystallizer represented schematically [15] 7

Figure 2-4: Swenson DTB crystallizer represented schematically [12] 8

Figure 2-5: Oslo-Krystal crystallizer represented schematically [12] 9

Figure 2-6: NiTech® reactor scheme [16] 9

Figure 2-7: Unit cell with its lattice parameters [9] 10

Figure 2-8: ASA unit cell [29] 11

Figure 2-9: Using Miller indices to index a crystal plane [9] 11

Figure 2-10: Surface sites of a crystal [18] 12

Figure 2-11: Screw dislocation on a crystal face [18] 12

Figure 2-12: Different habits of a crystal of the hexagonal crystal system [13] 14

Figure 2-13: Change of crystal habit and sphericity through temperature cycling if growth velocity is bigger than dissolution velocity [3] 15

Figure 2-14: Change of crystal habit and sphericity through temperature cycling if dissolution velocity is bigger than growth velocity [3] 16

Figure 2-15: Change of crystal habit through temperature cycling if steady-state growth faces are dissolved completely in the dissolution part [3] 16

Figure 4-1: Process flow diagram of cycling experiments 24

Figure 4-2: Part 1 of the experimental setup 25

Figure 4-3: Water baths, Part 2 of the experimental setup 25

Figure 4-4: Part 2 and 3 of the experimental setup 26

Figure 4-5: Total experimental setup 27

Figure 4-6: Schematic of a slug-flow consisting of air bubbles and flow compartments, called slugs, which contain the crystals [30] 28

Figure 4-7: Seed crystals 90-200 µm 29
Figure 4-8: Calculating the aspect ratio of particles.....35
Figure 4-9: PSD of seeds, using the filter conditions in QICPIC versus original data 37
Figure 4-10: Aspect ratio distribution of seeds, filtered versus original data 38
Figure 5-1: Product crystals of EtOH 99.8% from flask without water bath.....40
Figure 5-2: Product crystals of EtOH 99.8% from flask kept at constant temperature.....40
Figure 5-3: Product crystals cycled in isopropanol 41
Figure 5-4: Calibration curve of ASA in 1-hexanol.....42
Figure 5-5: Solubility curve of ASA in 1-hexanol 42
Figure 5-6: Product crystals cycled in a 70:30 vol% EtOH:n-heptane-mixture.....43
Figure 5-7: Calibration curve of ASA in n-heptane:EtOH-mixture.....44
Figure 5-8: Solubility curve of ASA in n-heptane:EtOH-mixture.....44
Figure 5-9: Solubility curves of the solvents chosen for the main experiments [32] 45
Figure 5-10: Seed-Habit stability.....46
Figure 5-11: Raman-Spectra of seed and product crystals cycled in EtOH 99.8% at ΔS_1 47
Figure 5-12: High speed camera images of cycling in EtOH 99.8% 48
Figure 5-13: SEM-image of pure seeds 49
Figure 5-14: SEM-image of EtOH 99.8% product crystals.....49
Figure 5-15: Results showing Q_3 over aspect ratio for chemical route ΔS_1-experiments. The error bars show the standard deviation of triple measurements. 50
Figure 5-16: Results showing q_3 over aspect ratio, chemical route ΔS_1.....51
Figure 5-17: CSD after cycling at ΔS_1 53
Figure 5-18: QICPIC signal test-images of chemical route ΔS_1 shape-changes; subimage b shows the seed crystals, a the product crystals cycled in 1-hexanol, c the product crystals cycled in isopropanol, d the product crystals cycled in EtOH 96% and e the product crystals cycled in EtOH 99%. 54
Figure 5-19: Results showing Q3 over aspect ratio, EtOH 99.8%, non-chemical route; error bars show standard deviation of triple measurements.....56

Figure 5-20: Results showing q3 over aspect ratio, EtOH 99.8%, non-chemical route 58

Figure 5-21: Results showing Q3 over aspect ratio, EtOH 96%, non-chemical route; error bars show standard deviation of triple measurements.....59

Figure 5-22: Results showing q3 over aspect ratio, EtOH 96%, non-chemical route 60

Figure 5-23: Results showing Q3 over aspect ratio, isopropanol, non-chemical route.....61

Figure 5-24: Results showing Q3 over aspect ratio, isopropanol, non-chemical route, comparison of ΔS_1- and ΔS_5-experiments; error bars show standard deviation of triple measurements.....62

Figure 5-25: Results showing q3 over aspect ratio, isopropanol, non-chemical route 63

Figure 5-26: Results showing Q3 over aspect ratio, 1-hexanol, non-chemical route; error bars show standard deviation of triple measurements.....64

Figure 5-27: Results showing q3 over aspect ratio, 1-hexanol, non-chemical route 65

Figure 6-1: Solvent-dependent results; error bars are indicating the standard deviation of triple measurements 72

Figure 6-2: Significantly different results for non-chemical route cycling in isopropanol; error bars are indicating the standard deviation of triple measurements.....73

Table of Tables

Table 4-1: Information about used solvents 19

Table 4-2: Characteristics of the used solvents.....20

Table 4-3: Equipment for cycling experiments.....21

Table 4-4: Equipment for product analysis 22

Table 4-5: Saturation-Settings for all solvents.....32

Table 4-6: Flow rate settings.....32

Table 4-7: Parameters used for theoretical residence time calculation.....33

Table 4-8: Settings for main experiments.....34

Table 5-1: Results of aspect ratio for chemical route ΔS1 experiments.....51

Table 5-2: Mean sphericity-values of chemical route ΔS_1 experiments.....52

Table 5-3: Averaged results of EtOH 99.8% non-chemical route experiments 56

Table 5-4: Significance of EtOH 99.8% non-chemical route experiments.....57

Table 5-5: Averaged results of EtOH 96% non-chemical route experiments 58

Table 5-6: Significance of EtOH 96% non-chemical route experiments.....59

Table 5-7: Averaged results of isopropanol non-chemical route experiments.....60

Table 5-8: Significance of isopropanol non-chemical route experiments (1).....61

Table 5-9: Significance of isopropanol non-chemical route experiments (2).....62

Table 5-10: Averaged results of 1-hexanol non-chemical route experiments 63

Table 5-11: Significance of 1-hexanol non-chemical route experiments.....64

Table 5-12: Chosen values for supersaturation-difference 67

Table 6-1: Supersaturation-Settings.....72

Appendix

Working Procedure

Working at the cycling-crystallization requires special knowledge of the system, which is very sensitive to even small changes in back-pressure, pressure-loss and temperature. A list was prepared that contains all issues needing particular attention.

Before the actual cycling process:

- The tube has to be washed thoroughly with pure solvent. No deposits may be left in it.
- The Peristaltic pump has to be calibrated.
- The tube has to be filled completely with saturated solution. No air bubbles should be in the tube.
- For comparison reasons, the same seeds have to be used in every experiment.
- ΔS has to be kept constant for different solvents.
- Before starting the slug flow, the same pressure as inside the 50m-system has to be achieved by pressure build-up inside the syringes of the syringe pump. For Isopropanol about 12-15 ml have to be pumped before starting to insert the air-bubbles, for EtOH about 15-20 ml, for 1-Hexanol almost 30 ml.

After the start of the cycling process:

- Slugs have to be evenly distributed and may not split up into many, many small ones, which produce too much back-pressure.
- The flask containing the starting suspension has to be open in order to ensure atmospheric pressure inside the flask.
- The temperature has to be recorded and controlled thoroughly. The water bath temperature has to be checked every few minutes.
- It has to be checked continuously, if seed are passing through the pump tubing in order not to plug it.
- A magnetic stir bar has to be used in the flask collecting the product suspension for the Lixell measurement.
- Frit and vacuum pump have to be prepared, if samples for microscopy are to be taken.

Comparison of Chemical Route Cycling Experiments at ΔS2

The chemical route changes can also be evaluated for the bigger supersaturation-difference ΔS_2. Figure Ap-1 shows the resulting curves of those experiments. Compared to the diagram at ΔS_1, the curves lie farther from each other.

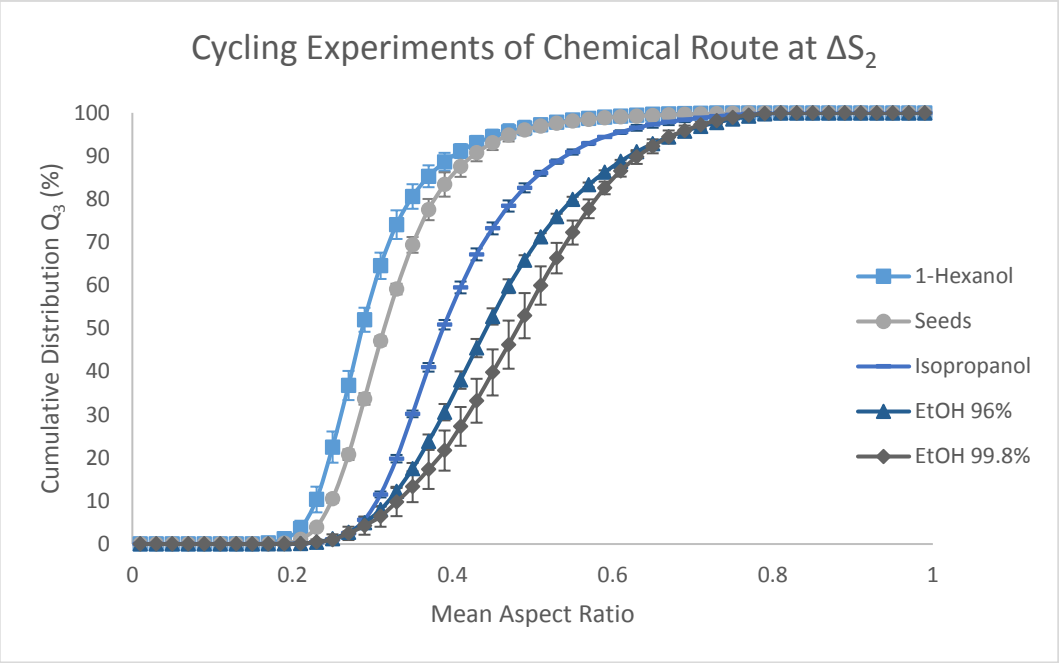

Figure Ap-1: Results showing Q_3 over aspect ratio, chemical route ΔS_2